

Tommy Kunhung Kim  
September 2001  
Applied Mathematics

A Modified Smagorinsky Subgrid Scale Model for the Large Eddy Simulation of  
Turbulent Flow

**Abstract**

In the field of Large Eddy Simulation, the Smagorinsky subgrid scale model (in some form) is the most commonly accepted and used subgrid scale model. The purpose of this paper is to address the main weakness of the Smagorinsky model, its poor performance near the wall. The goal is to establish a model that corrects the Smagorinsky model near the walls while at the same time minimizing the computational overhead. A version the Dynamic Subgrid Scale model is also incorporated into the finite element code to facilitate comparisons with the new model near the walls.

One of the unique characteristics of Large Eddy Simulations as compared to other methods of dealing with turbulent flows is the idea of filtering. In this paper we define what a filter is and also address an issue related to filters; the error that results when the filtering and differential operations are interchanged. This error is studied under the context of the Finite Element Method which allows us to focus on the function being filtered rather than the filter kernel function, which has been the usual approach in studying this error.

---

# A Modified Smagorinsky Subgrid Scale Model for the Large Eddy Simulation of Turbulent Flow

BY

Tommy Kunhung Kim

B.A. (California State University, Fullerton) 1990  
M.A. (California State University, Fullerton) 1992

DISSERTATION

Submitted in partial satisfaction of the requirements for the degree of

DOCTOR OF PHILOSOPHY

in

Applied Mathematics

in the

OFFICE OF GRADUATE STUDIES

of the

UNIVERSITY OF CALIFORNIA

DAVIS

Approved: \_\_\_\_\_

\_\_\_\_\_

\_\_\_\_\_

Committee in Charge

2001

## **Abstract**

In the field of Large Eddy Simulation, the Smagorinsky subgrid scale model (in some form) is the most commonly accepted and used subgrid scale model. The purpose of this paper is to address the main weakness of the Smagorinsky model, its poor performance near the wall. The goal is to establish a model that corrects the Smagorinsky model near the walls while at the same time minimizing the computational overhead. A version the Dynamic Subgrid Scale model is also incorporated into the finite element code to facilitate comparisons with the new model near the walls.

One of the unique characteristics of Large Eddy Simulations as compared to other methods of dealing with turbulent flows is the idea of filtering. In this paper we define what a filter is and also address an issue related to filters; the error that results when the filtering and differential operations are interchanged. This error is studied under the context of the Finite Element Method which allows us to focus on the function being filtered rather than the filter kernel function, which has been the usual approach in studying this error.

# Contents

<b>1</b>	<b>Introduction</b>	<b>1</b>
<b>2</b>	<b>LES</b>	<b>3</b>
2.1	Filtering . . . . .	3
2.2	Filtering and FEM . . . . .	10
2.3	Governing Equations . . . . .	17
2.4	Subgrid Scale Models . . . . .	20
2.4.1	Smagorinsky Model . . . . .	21
2.4.2	Dynamic Subgrid Scale Model . . . . .	25
2.4.3	Modified Smagorinsky Model . . . . .	28
<b>3</b>	<b>Channel Flow</b>	<b>31</b>
3.1	Computational Parameters . . . . .	31
3.2	Constant Flow Rate . . . . .	33
3.3	Numerical Results . . . . .	37
<b>4</b>	<b>Flow over a Backward Facing Step</b>	<b>47</b>
4.1	Computational Parameters . . . . .	47
4.2	Numerical Results . . . . .	47
<b>5</b>	<b>Computer Software</b>	<b>58</b>
<b>6</b>	<b>Conclusions</b>	<b>59</b>

<b>A Filter/Derivative Interchange Error</b>	<b>64</b>
<b>B The Effect of Double Filtering</b>	<b>68</b>
B.1 Gaussian Filter . . . . .	68
B.2 Top-Hat Filter . . . . .	71

## 1 Introduction

In the study of turbulence, three distinct computational approaches have been developed to simulate turbulent flows. Direct numerical simulation (DNS), as the name implies, is the most straight forward approach to the simulation of turbulent flows. The DNS approach is to simply solve the Navier-Stokes equations using some numerical method. The problem with this approach is that to successfully solve the Navier-Stokes equations, the computational domain must be large enough to contain the largest scales of motion,  $L$ , while the grid resolution must also be fine enough to resolve the smallest scales, which are of the order of the Kolmogorov microscale,  $\eta = (\nu^3/\epsilon)^{1/4}$ , where  $\eta$  is the dissipation rate per unit mass and  $\nu$  is the kinematic viscosity. So, the number of grid points necessary in each direction can be estimated as  $\frac{L}{\eta}$  and using the well established relationship between  $\frac{L}{\eta}$  and the Reynolds number,  $Re$ , (see Tennekes and Lumely, [26]) we have that

$$N = \left(\frac{L}{\eta}\right)^3 \sim Re^{\frac{9}{4}},$$

where  $N$  is the number of grid points. Hence, it is clear that DNS is only practical for low Reynolds number flows. At the other end of the spectrum from the DNS approach is the Reynolds averaged simulations (RAS). In RAS, the flow (velocity field and pressure for incompressible flows) is broken up into a statistically steady (mean) portion and fluctuations. The mean flow is then solved for, while the effects of the fluctuations on the flow are modelled. By modeling the fluctuation effects, the RAS approach models all the turbulent interactions whereas the DNS approach completely

resolves them. One of the main stumbling blocks for RAS is that no one model has been found for the fluctuation effects that can be used for all turbulent flows. It seems unlikely that such a model would exist given the complexity of turbulent flows and the fact that turbulence is a property of the flow rather than the fluid. The third approach to the computation of turbulent flows, known as Large-Eddy simulation (LES), is often viewed as the intermediary approach between DNS and RAS. The motivation behind LES is that since the large energy carrying eddies are highly influenced by the boundary conditions, it should be computationally resolved, while the small eddies or unresolved scales are modelled. It is hoped that since the small eddies are more homogeneous and isotropic, a simpler and more universal model can be used for the unresolved scales as compared to the RAS models.

The objective of this study is to develop a new model for the unresolved scales that overcomes some of the problems associated with the established models, which are discussed in the coming sections. This study is based on and, in many ways, an extension of the work begun by Rose McCallen [19] in which a LES method is incorporated into a finite element code. In her study, a classical model for the unresolved scales developed by Smagorinsky [25] was used to simulate the channel and backward facing step flows in two dimensions. In the present study, this model plus a version of a newer model first developed by Germano, Piomelli, Moin, and Cabbot [6] and our own model based on the Smagorinsky model are used to simulate the channel and backward facing step flows in three dimensions.

## 2 LES

### 2.1 Filtering

In LES, the underlying principle is to separate the large eddies, which are computationally resolved, from the small, which are modelled. This partitioning of the scales is accomplished by filtering, in the case of incompressible flow, the velocity field,  $\mathbf{u}$ , and pressure,  $P$ . Following the work of Leonard [16], if  $f(\mathbf{x})$  is a function that contains all the scales, then the filter of  $f$ , denoted as  $\bar{f}$ , is defined as the convolution of  $f$  with a filter function  $G(\mathbf{x})$ .

$$\bar{f}(\mathbf{x}) = \int_{\Gamma} G(\mathbf{x} - \mathbf{s}) f(\mathbf{s}) d\mathbf{s} \quad (1)$$

where  $\Gamma$  is the flow volume,  $G$  is normalized so that

$$\int_{\Gamma} G(\mathbf{s}) d\mathbf{s} = 1,$$

and  $G(-x) = G(x)$ . This is necessary to insure that when  $f$  is constant that  $\bar{f} = f$ .

Some common filters are the following:

- Top-Hat filter

$$G(\mathbf{x} - \mathbf{s}) = \begin{cases} \frac{1}{\Delta_f^3} & \text{for } |\mathbf{x} - \mathbf{s}| < \frac{\Delta_f}{2} \\ 0 & \text{otherwise} \end{cases}$$

where  $\Delta_f$  is the filter size. If  $\mathbf{u}$  is the velocity field, then the filter of  $\mathbf{u}$ , using

the Top-Hat filter, is

$$\bar{\mathbf{u}}(\mathbf{x}) = \frac{1}{\Delta_f^3} \int_{-\frac{\Delta_f}{2}}^{\frac{\Delta_f}{2}} \mathbf{u}(\mathbf{x} + \mathbf{s}) d\mathbf{s}$$



which is equivalent to cell volume averaging of Deardorff [2]. Now, the Fourier transform of  $\bar{\mathbf{u}}(\mathbf{x})$  is

$$\hat{\mathbf{u}}(\mathbf{k}) = \left[ \prod_{i=1}^3 \frac{\sin\left(k_i \frac{\Delta_f}{2}\right)}{k_i \frac{\Delta_f}{2}} \right] \hat{\mathbf{u}}(\mathbf{k}), \quad (2)$$

where  $\hat{\mathbf{u}}(\mathbf{k})$  is the Fourier transform of  $\mathbf{u}$  (see Kwak *et al.* [14].) So, we see that the spectrum of the filtered field contains components of all wave numbers. This implies that the Top-Hat filter will not filter out all the small scales of the flow. Also, the wave numbers for which the coefficient of  $\hat{\mathbf{u}}(\mathbf{k})$  in Eqn. (2) is zero lead to the inverse transform being singular. This means that it is not possible to obtain the actual spectrum  $\hat{\mathbf{u}}(\mathbf{k})$  from the filtered one,  $\hat{\mathbf{u}}(\mathbf{k})$ . So the Top-Hat filter is not appropriate when spectral results are sought.

- Gaussian filter

$$G(\mathbf{x} - \mathbf{s}) = \left( \frac{6}{\pi \Delta_f^2} \right)^{\frac{3}{2}} \exp\left( \frac{-6(\mathbf{x} - \mathbf{s})^2}{\Delta_f^2} \right)$$

According to Rogallo and Moin [24], the Gaussian filter is a good filter choice for filtering in the homogeneous directions because it provides a smooth transition between the resolved and subgrid (unresolved) scales and is positive definite in both the physical and wave space. Kwak *et al.* [14] showed that the Gaussian filter results in a filtered field that captures most of the large scale motion while most of the small scale motions are removed. This ability of the Gaussian filter to separate the large and small scales, gives it a desirable property for a filter in LES. The one obvious flaw or weakness of this filter is that it does not have

a compact domain. Hence, its use in non-homogeneous, wall bounded flows is questionable at best.

- Sharp-Cutoff filter

$$G(x) = \prod_{i=1}^3 \frac{\sin\left(\frac{\pi(x_i - s_i)}{\Delta_f}\right)}{\pi(x_i - s_i)}$$

Just as the Top-Hat filter has compact support in grid coordinates, the Sharp-Cutoff filter has compact support in the wave space. Also, just as the Top-Hat filter loses its compact support when transformed into the wave space, the Sharp-Cutoff filter loses its compact support when going from the wave space to grid coordinates. So, like the Gaussian filter, it is not appropriate for non-homogeneous, wall bounded flows.

Although Leonard's definition for filtering is generally accepted, two distinct approaches to the application of the filter have been developed. These are mainly influenced by the flow under study and the numerical technique used to solve the flow problem. In the case of homogeneous turbulence, the use of spectral methods facilitates the use of an explicit filter. However, in using finite difference methods, usually for non-homogeneous flows, the filter is assumed to be implicitly defined by the discretization. An example of this implicit filter is given by Rogallo and Moin, [24], where they note that the second-order central-difference of a function  $f$  is the derivative of the filter of  $f$ :

$$\frac{f(x + \Delta) - f(x - \Delta)}{2\Delta} = \frac{d}{dx} \left[ \frac{1}{2\Delta} \int_{x-\Delta}^{x+\Delta} f(s) ds \right] = \frac{d\bar{f}}{dx},$$

where the filter used is the Top–Hat filter. Some of the reasons for using an implicit filter rather than explicitly applying a filter are the following: the difficulty of actually applying a filter; the reduction in grid resolution resulting from the fact that in finite differencing, the function is only defined at the grid nodal points and so any filtering would require at least two nodal points (i. e. just like the pressure, the differencing would be done using the grid nodes, but the filtered value would be at the cell center); and finally, finite difference schemes are usually used for non–homogenous wall bounded flows which usually have anisotropic grids (since the filter width will most likely depend on the grid, this means that the filter width would be a function of location unlike the homogeneous case where the filter width remains constant. This leads to further difficulties, as will be discussed below.)

In applying a filter, Eqn. (1), to get the LES equations, a question that arises is whether or not the derivative operator and filtering are interchangeable, i. e. is the derivative of the filter equal to the filter of the derivative. The answer will depend on the flow under study. In the case of homogeneous turbulence, where the scales of the large and small eddies do not depend on the location in space, there would be no reason to use anything but a constant filter width,  $\Delta$ . So, assuming that  $G \rightarrow 0$  as  $t \rightarrow \infty$  and using the 1–dimensional case for notational simplicity (with the extension into higher dimensions following in the usual way),

$$\begin{aligned} \frac{\partial \bar{f}(x)}{\partial x} &= \frac{\partial}{\partial x} \int_{-\infty}^{\infty} f(s)G(x-s) ds \\ &= \int_{-\infty}^{\infty} f(s) \frac{\partial}{\partial x} G(x-s) ds \end{aligned}$$

$$\begin{aligned}
&= \int_{-\infty}^{\infty} \frac{\partial}{\partial s} f(s) G(x-s) ds \\
&= \frac{\partial f}{\partial x},
\end{aligned}$$

where integration by parts and the fact that if  $\xi = x - s$ , then

$$\frac{\partial}{\partial x} G = \frac{d}{d\xi} G \frac{\partial \xi}{\partial x} = G'$$

and

$$\frac{\partial}{\partial s} G = \frac{d}{d\xi} G \frac{\partial \xi}{\partial s} = -G'$$

were used in the above derivation. So, under the assumptions made above, the derivative and filtering operations are interchangeable in the case of uniform filter width which occurs in homogeneous turbulence.

For the non-homogeneous wall bounded flow, since the scale of the large and small eddies will depend on position relative to the wall, it is clear that the filter width must be a function of location. To emphasize this, we rewrite the definition of filtering, Eqn. (1), as

$$\bar{f}(\mathbf{x}) = \frac{1}{\Delta(\mathbf{x})} \int_{\Gamma} G\left(\frac{\mathbf{x}-\mathbf{s}}{\Delta(\mathbf{x})}\right) f(\mathbf{s}) ds. \quad (3)$$

It can be shown by simply carrying out the differentiation, that the derivative and filtering operations are not, in general, interchangeable. For this reason, there is ongoing research to find filters that reduce the error in interchanging the derivative and filtering operations (Germano [5]; Ghosal and Moin [7]; van der Ven [28]; Najjar and Tafti [21]; Vasilyev and Lund [30] [29]; and Marsden, Vasilyev and Moin [17].) However, as of the time of this report, there is no compelling evidence to indicate

the best filter choice. As mentioned before, in using the finite difference methods, researchers often assumed an implicit filter. The issue of the interchange of filter and differentiation was then bypassed by assuming that just as when using the Reynolds Average method, one assumes that all turbulent behavior is captured by the model for the Reynolds stress, all of the effects of filtering were assumed to be captured by the sub-grid scale model. More recently, there have been some studies where an explicit discrete filter is used instead of the implicit filter (Najjar et al. [21]; Vasilyev et al. [30] [29]; and Marsden et al. [17].) However, as Vasilyev pointed out, there is more work to be done before any conclusions can be drawn about the effectiveness of the discrete filter.

In the case of the Top-Hat filter, in 1-dimension, the filter of  $f$  is

$$\bar{f} = \frac{1}{\Delta(x)} \int_{x-\frac{\Delta(x)}{2}}^{x+\frac{\Delta(x)}{2}} f(s) ds$$

and

$$\frac{\partial \bar{f}}{\partial x} = \frac{1}{\Delta(x)} \int_{x-\frac{\Delta(x)}{2}}^{x+\frac{\Delta(x)}{2}} f'(s) ds = \frac{f(x + \frac{\Delta(x)}{2}) - f(x - \frac{\Delta(x)}{2})}{\Delta(x)}.$$

Using the above, we calculate the derivative of the filter of  $f$  as follows:

$$\begin{aligned} \frac{\partial \bar{f}}{\partial x} &= \frac{\partial}{\partial x} \left[ \frac{1}{\Delta(x)} \int_{x-\frac{\Delta(x)}{2}}^{x+\frac{\Delta(x)}{2}} f(s) ds \right] \\ &= -\frac{\Delta'(x)}{\Delta^2(x)} \int_{x-\frac{\Delta(x)}{2}}^{x+\frac{\Delta(x)}{2}} f(s) ds + \frac{1}{\Delta(x)} \left[ \left(1 + \frac{\Delta'(x)}{2}\right) f\left(x + \frac{\Delta(x)}{2}\right) \right] \\ &\quad - \frac{1}{\Delta(x)} \left[ \left(1 - \frac{\Delta'(x)}{2}\right) f\left(x - \frac{\Delta(x)}{2}\right) \right] \\ &= \frac{\partial f}{\partial x} - \frac{\Delta'(x)}{\Delta(x)} \bar{f} + \frac{\Delta'(x)}{2\Delta(x)} \left[ f\left(x + \frac{\Delta(x)}{2}\right) + f\left(x - \frac{\Delta(x)}{2}\right) \right]. \end{aligned}$$

By the trapezoidal rule,

$$\bar{f}(x) = \frac{1}{\Delta(x)} \int_{x-\frac{\Delta(x)}{2}}^{x+\frac{\Delta(x)}{2}} f(s) ds = \frac{1}{2} \left[ f\left(x + \frac{\Delta(x)}{2}\right) + f\left(x - \frac{\Delta(x)}{2}\right) \right] + O(\Delta^2 f'').$$

So, using this and the previous equation, we get

$$\frac{\partial \bar{f}}{\partial x} - \overline{\frac{\partial f}{\partial x}} = -\frac{\Delta'(x)}{\Delta(x)} \bar{f} + \frac{\Delta'(x)}{\Delta(x)} [\bar{f} - O(\Delta^2 f'')] = O(\Delta' \Delta f'').$$

Since we choose our filter width,  $\Delta$ , to be the length of our grid element and the grids that we use are graded near the wall,  $\Delta' \neq 0$  and so the above shows that the magnitude of the error in the interchange of the derivative and filtering operator is dependent on the derivative of the filter width,  $\Delta'$ . To obtain a better perspective on the implications of the interchange error, we first rewrite it as

$$\frac{\partial \bar{f}}{\partial x} - \overline{\frac{\partial f}{\partial x}} = O\left(\frac{\Delta'}{\Delta} \Delta^2 f''\right).$$

It is clear that if  $\frac{\Delta'}{\Delta} = O(1)$ , then the interchange error is second order. Now, assuming that

$$\frac{\Delta'}{\Delta} = M$$

for some constant,  $M$ , we get

$$\Delta = C e^{Mx}$$

where  $C$  is a constant. Hence, if the filter width behaves like the exponential function, then the error in the interchange of filtering and differentiation is second order, using the Top-Hat filter.

## 2.2 Filtering and FEM

One of the advantages and/or characteristics of the Finite Element Method (FEM) over the Finite Difference Method is that instead of producing a solution over a discrete set of points, it produces a continuous approximation of the actual solution. In fact the general shape of the approximation function is known and chosen by the user via the shape functions before the actual computations begin. This knowledge of the general shape of the function being filtered naturally leads to the question of how this information can be used or effects the analysis of the error in the interchange of filtering and differentiation.

We begin by modifying the definition of filtering, for the one dimensional case, in the following way.

$$\bar{u}(x) = \frac{1}{\Delta(x)} \int_{x-\frac{\Delta(x)}{2}}^{x+\frac{\Delta(x)}{2}} G\left(\frac{x-s}{\Delta(x)}\right) u_e(s) ds$$

where  $u_e(x)$  is the finite element representation of  $u(x)$ . Now using the transformation  $y = \frac{x-s}{\Delta(x)}$ , the above becomes

$$\bar{u}(x) = \int_{-\frac{1}{2}}^{\frac{1}{2}} G(y) u_e(x - y\Delta(x)) dy$$

Differentiating this, we get

$$\frac{d\bar{u}}{dx}(x) = \int_{-\frac{1}{2}}^{\frac{1}{2}} G(y) u'_e(x - y\Delta(x)) (1 - y\Delta'(x)) dy. \quad (4)$$

Note that in general  $u_e(x)$  is only required to be continuous rather than continuously differentiable. It is however continuously differentiable in each element. So we use

the above notation with the understanding that

$$\begin{aligned}
\int_{-\frac{1}{2}}^{\frac{1}{2}} G(y)u'_e(x - y\Delta(x))(1 - y\Delta'(x)) dy &= \int_{-\frac{1}{2}}^{x_1} G(y)u'_{e_1}(x - y\Delta(x))(1 - y\Delta'(x)) dy \\
&+ \int_{x_1}^{x_2} G(y)u'_{e_2}(x - y\Delta(x))(1 - y\Delta'(x)) dy \\
&+ \dots \\
&+ \int_{x_n}^{\frac{1}{2}} G(y)u'_{e_n}(x - y\Delta(x))(1 - y\Delta'(x)) dy
\end{aligned}$$

where  $(x_i, x_{i+1})$  represents the transformed elements contained in the support for the filter. Note that

$$\overline{\frac{du}{dx}}(x) = \int_{-\frac{1}{2}}^{\frac{1}{2}} G(y)u'_e(x - y\Delta(x)) dy$$

and so using this in Eqn. (4) we get our error term

$$\left| \frac{d\bar{u}}{dx}(x) - \overline{\frac{du}{dx}}(x) \right| = \left| \Delta'(x) \int_{-\frac{1}{2}}^{\frac{1}{2}} yG(y)u'_e(x - y\Delta(x)) dy \right| \quad (5)$$

If we assume a linear shape function then

$$u_{e_i}(x) = \alpha_i + \beta_i(x)$$

for  $x \in \Omega_i$  where  $\Omega_i$  is the  $i$ -th element. We define the filter width  $\Delta(x)$  to be twice the width of the smaller of the two intervals containing the nodal point  $x$ . This allows us to separate the error term, Eqn. (5), in terms of each element as follows:

$$\left| \frac{d\bar{u}}{dx}(x) - \overline{\frac{du}{dx}}(x) \right| = \beta_1\Delta'(x) \int_0^{\frac{1}{2}} yG(y) dy + \beta_2\Delta'(x) \int_{-\frac{1}{2}}^0 yG(y) dy.$$

The above would seem to indicate that the error in the interchange is of order  $\Delta'(x)$ .

This would be the case if the filter width is defined such that a change in the filter



width does not imply a change in the element width. However, the above definition of the filter width not only involves  $x$  but also the element width, which we denote  $\Delta_{e_i}(x)$ . Now, we note that

$$\beta_1 = \frac{u(x) - u(x - \Delta_{e_1}(x))}{\Delta_{e_1}(x)} = u'(x) + O(\Delta_{e_1}(x))$$

and

$$\beta_2 = u'(x) + O(\Delta_{e_2}(x))$$

where if we let  $x = x_n$ , then  $\Delta_{e_1}(x) = x_n - x_{n-1}$  and  $\Delta_{e_2}(x) = x_{n+1} - x_n$  for gradings of  $x_n$  that increase with  $n$ . Since  $G$  is defined as an even function we have

$$\int_0^{\frac{1}{2}} yG(y) dy = - \int_{-\frac{1}{2}}^0 yG(y) dy.$$

So

$$\begin{aligned} \left| \frac{d\bar{u}}{dx}(x) - \overline{\frac{du}{dx}}(x) \right| &= \left| (\beta_2 - \beta_1)\Delta'(x) \int_0^{\frac{1}{2}} yG(y) dy \right| \\ &= \left| (O(\Delta_{e_2}(x)) - O(\Delta_{e_1}(x)))\Delta'(x) \int_0^{\frac{1}{2}} yG(y) dy \right| \\ &= O(\Delta_e(x)\Delta'(x)) \end{aligned}$$

where for practical problems the order of the local element widths are the same, i. e.  $O(\Delta_{e_1}(x)) = O(\Delta_{e_2}(x)) = O(\Delta_e(x))$ . Furthermore, if we assume a smooth exponential grading such that  $O(\Delta'(x)) = O(\Delta(x))$ , then the interchange error is second order,

$$\left| \frac{d\bar{u}}{dx}(x) - \overline{\frac{du}{dx}}(x) \right| = O(\Delta_e^2(x)).$$

For a quadratic shape function, we have

$$u_{e_i}(x) = \alpha_i + \beta_i x + \gamma_i x^2$$

for  $x \in \Omega_i$ . Again, using the above filter definition, the interchange error is

$$\begin{aligned} \left| \frac{d\bar{u}}{dx}(x) - \overline{\frac{du}{dx}}(x) \right| &= (\beta_1 + 2\gamma_1 x) \Delta'(x) \int_0^{\frac{1}{2}} y G(y) dy \\ &\quad - 2\gamma_1 \Delta(x) \Delta'(x) \int_0^{\frac{1}{2}} y^2 G(y) dy \\ &\quad + (\beta_2 + 2\gamma_2 x) \Delta'(x) \int_{-\frac{1}{2}}^0 y G(y) dy \\ &\quad - 2\gamma_2 \Delta(x) \Delta'(x) \int_{-\frac{1}{2}}^0 y^2 G(y) dy \end{aligned}$$

Note that in FEM,  $u_{e_i}(x) = \alpha_i + \beta_i x + \gamma_i x^2$  is exact at each nodal point, i. e.  $u_{e_i}(x_n) = u(x_n)$ . So, using the above definition of  $\Delta_{e_i}(x)$ , we have the following first order approximation of the derivative of  $u$ :

$$\begin{aligned} u'(x) &= \frac{u(x) - u(x - \Delta_{e_1}(x))}{\Delta_{e_1}(x)} + O(\Delta_{e_1}(x)) \\ &= \frac{u_{e_1}(x) - u_{e_1}(x - \Delta_{e_1}(x))}{\Delta_{e_1}(x)} + O(\Delta_{e_1}(x)) \\ &= \frac{\alpha_1 + \beta_1 x + \gamma_1 x^2 - [\alpha_1 + \beta_1(x - \Delta_{e_1}(x)) + \gamma_1(x - \Delta_{e_1}(x))^2]}{\Delta_{e_1}(x)} + O(\Delta_{e_1}(x)) \\ &= \beta_1 + 2\gamma_1 x - \gamma_1 \Delta_{e_1}(x) + O(\Delta_{e_1}(x)) \end{aligned}$$

So

$$\beta_1 + 2\gamma_1 x = u'(x) + O(\Delta_{e_1}(x))$$

and using a similiar argument, we also have

$$\beta_2 + 2\gamma_2 x = u'(x) + O(\Delta_{e_2}(x)).$$

Hence, using the symmetry of  $G$  as in the linear case, the interchange error is again

$$\left| \frac{d\bar{u}}{dx}(x) - \overline{\frac{du}{dx}}(x) \right| = O(\Delta_\epsilon(x)\Delta'(x)).$$

We now show that for any polynomial shape function, the interchange error is of order  $O(\Delta_\epsilon(x)\Delta'(x))$ . Consider a general  $n$ -th order polynomial shape function

$$u_{e_j}(x) = \sum_{i=0}^n \alpha_{i,j} x^i.$$

Note that

$$u'_{e_j}(x) = \sum_{i=1}^n i\alpha_{i,j} x^{i-1}.$$

So the interchange error, Eqn. (5), can be written as

$$\begin{aligned} \left| \frac{d\bar{u}}{dx}(x) - \overline{\frac{du}{dx}}(x) \right| &= \left| \Delta'(x) \int_{-\frac{1}{2}}^0 yG(y) \sum_{i=1}^n i\alpha_{i,1}(x - y\Delta(x))^{i-1} dy \right. \\ &\quad \left. + \Delta'(x) \int_0^{\frac{1}{2}} yG(y) \sum_{i=1}^n i\alpha_{i,2}(x - y\Delta(x))^{i-1} dy \right|. \end{aligned}$$

We can ignore any term that has  $\Delta(x)$  since they will be of order  $O(\Delta(x)\Delta'(x))$  or higher. So, using the Binomial Theorem and the fact that  $G$  is symmetric, the interchange error above can be rewritten as

$$\begin{aligned} \left| \frac{d\bar{u}}{dx}(x) - \overline{\frac{du}{dx}}(x) \right| &= \left| \Delta'(x) \left[ \left( \sum_{i=1}^n i\alpha_{i,2} x^{i-1} \right) - \left( \sum_{i=1}^n i\alpha_{i,1} x^{i-1} \right) \right] \int_0^{\frac{1}{2}} yG(y) dy \right. \\ &\quad \left. + O(\Delta(x)\Delta'(x)) \right| \end{aligned} \quad (6)$$

Now, as in the quadratic case, we note that the interpolating polynomial function is exact at each nodal point, i. e.  $u_{e_j}(x_n) = u(x_n)$ . So

$$u'(x) + O(\Delta_{e_1}(x)) = \frac{u(x) - u(x - \Delta_{e_1}(x))}{\Delta_{e_1}(x)}$$

$$\begin{aligned}
&= \frac{u_{e_1}(x) - u_{e_1}(x - \Delta_{e_1}(x))}{\Delta_{e_1}(x)} \\
&= \frac{\sum_{i=0}^n \alpha_{i,1} x^i - \sum_{i=0}^n \alpha_{i,1} (x - \Delta_{e_1}(x))^i}{\Delta_{e_1}(x)}
\end{aligned}$$

Again, using the Binomial Theorem, we rewrite the above as

$$u'(x) + O(\Delta_{e_1}(x)) = \frac{\sum_{i=0}^n \alpha_{i,1} x^i - \sum_{i=0}^n \alpha_{i,1} \sum_{j=0}^i \binom{i}{j} x^j (-\Delta_{e_1}(x))^{i-j}}{\Delta_{e_1}(x)}$$

Note that the terms that do not have any factor of  $\Delta_{e_1}(x)$  cancel out which leaves the terms with a factor of just  $\Delta_{e_1}(x)$  as the lowest order terms. So, collecting these terms, the above can be rewritten as

$$u'(x) + O(\Delta_{e_1}(x)) = \sum_{i=1}^n i \alpha_{i,1} x^{i-1}.$$

Using same argument as above only with a first order forward differencing scheme instead of the backward differencing scheme, we get

$$u'(x) + O(\Delta_{e_2}(x)) = \sum_{i=1}^n i \alpha_{i,2} x^{i-1}.$$

Using the above in Eqn. (6), we get

$$\left| \frac{d\bar{u}}{dx}(x) - \overline{\frac{du}{dx}}(x) \right| = O(\Delta_e(x) \Delta'(x))$$

where again we assume that the filter and element widths are of the same order, i. e.  $O(\Delta(x)) = O(\Delta_{e_i}(x)) = O(\Delta_e(x))$ . So if we assume that the grading of the elements is smooth enough such that  $O(\Delta'(x)) = O(\Delta(x))$  then the error in the interchange of differentiation and filtering is second order for any polynomial interpolation of degree one or greater.

Appendix A presents the results of a computational experiment that verifies the above results for the case of linear and quadratic shape functions. Note that since the FEM is applied to solve the filtered equations, the above filtering technically only applies to filtering a filtered quantity. This is true for any explicit filter of  $u$  since the only values of  $u$  that are available are those that are obtained from the numerical method. But the numerical method is used to solve the LES or filtered equations and not the original, as discussed in the following section. Hence, to be completely consistent, an explicit filter can only be applied in a double filtering situation such as when using the Dynamic Subgrid Scale model discussed below. It would seem that to be consistent the initial filtering needs to be introduced in one of two ways. One, it can be introduced by a term representing the derivative/filter interchange error or this error can be ignored by using a filter whose interchange error is of the same order as the numerical scheme. Note that this error must be derived using the original vector field  $u$  and should avoid any reference to the computed  $u$ . Also, this filter would not be applied directly to the numerical solution but should instead be applied to the experimental or DNS data for comparison with the LES data. The second and ideal place to introduce the filter effect would be the SGS model since the filter determines the scales that are in the system.

### 2.3 Governing Equations

The set of equations that govern the motion of (Newtonian) fluids are known collectively as the Navier–Stokes equations. In the case of incompressible fluids with uniform density, the non–dimensionalized equations are

$$\begin{cases} \frac{\partial u_\alpha}{\partial x_\alpha} = 0 \\ \frac{\partial u_\alpha}{\partial t} + \frac{\partial}{\partial x_\beta}(u_\alpha u_\beta) = -\frac{\partial P}{\partial x_\alpha} + \frac{1}{Re} \frac{\partial^2}{\partial x_\beta^2} u_\alpha, \end{cases}$$

where we use the standard tensor notation of repeated indices indicating summation,  $P = \frac{P}{\rho}$ , and  $Re = \frac{UL}{\nu}$  with  $U$  being the characteristic velocity,  $L$  being the characteristic length, and  $\nu$  being the kinematic viscosity. Now, assuming that the error in the interchange of filtering and differentiation can be ignored (i. e.  $\overline{\frac{\partial f}{\partial x}} = \frac{\partial \bar{f}}{\partial x}$ ), the filtered Navier–Stokes equations are

$$\begin{cases} \frac{\partial \bar{u}_\alpha}{\partial x_\alpha} = 0 \\ \frac{\partial \bar{u}_\alpha}{\partial t} + \frac{\partial}{\partial x_\beta}(\overline{u_\alpha u_\beta}) = -\frac{\partial \bar{P}}{\partial x_\alpha} + \frac{1}{Re} \frac{\partial^2}{\partial x_\beta^2} \bar{u}_\alpha. \end{cases} \quad (7)$$

By filtering the equations above, we have introduced a new unknown term,  $\overline{u_\alpha u_\beta}$ , but no new equation. This means that the system of equations is now underdetermined. This is known as the closure problem, which is also encountered by researchers using RAS. In fact, the Reynolds Averaged Navier–Stokes equations look very much like the filtered Navier–Stokes equation above (Eqn. (7) with the  $\bar{\cdot}$  replaced by  $\langle \cdot \rangle$ , which represents the Reynolds averaging operator.) The difference is in how the  $\bar{\cdot}$  (and/or  $\langle \cdot \rangle$ ) is defined. In LES, the decomposition of variables is in terms of the large scales and small, i. e.  $u = \bar{u} + u'$  where  $\bar{u}$  is the large scale component of  $u$  and

$u'$  is the small or sub-scale component. From the definition of filtering, Eqn. (1), it is clear that in general  $\overline{\overline{u}} \neq \overline{u}$ , unless of course  $u$  is constant or the filter used is the Sharp-Cutoff. This means that, in general,  $\overline{u'} \neq 0$ . In the Reynolds Averaging method, the decomposition is in terms of the statistical mean and fluctuations with 0 mean. So if we write  $u = \langle u \rangle + u'$  then  $\langle \langle u \rangle \rangle = \langle u \rangle$  and  $\langle u' \rangle = 0$ . This difference, in the interpretation of the decomposition of variables, leads to a very different interpretation, both physically and mathematically, of Eqn. (7). In either case, note that the interaction between large and small scales ( $\overline{u}$  and  $u'$ ) or mean and fluctuations ( $\langle u \rangle$  and  $u'$ ) must occur in the  $\overline{u_\alpha u_\beta}$  term of Eqn. (7). As this work is based on LES, our focus will be on the closure problem as it relates to LES.

To deal with the closure problem, the above filtered equations, Eqn. (7), are rewritten as

$$\begin{cases} \frac{\partial \overline{u}_\alpha}{\partial x_\alpha} = 0 \\ \frac{\partial \overline{u}_\alpha}{\partial t} + \frac{\partial}{\partial x_\beta} (\overline{u}_\alpha \overline{u}_\beta) = -\frac{\partial \overline{P}}{\partial x_\alpha} - \frac{\partial}{\partial x_\beta} \tau_{\alpha\beta} + \frac{1}{Re} \frac{\partial^2}{\partial x_\beta^2} \overline{u}_\alpha \end{cases} \quad (8)$$

where

$$\tau_{\alpha\beta} = \overline{u_\alpha u_\beta} - \overline{u}_\alpha \overline{u}_\beta$$

is called the subgrid scale (SGS) Reynolds stress. The SGS Reynolds stress in LES is similar to the Reynolds stress in RAS in that in both cases the the unresolved scales,  $u'$  (small eddies in LES and turbulent fluctuations in RAS,) are viewed as producing stresses in the resolved scales (large eddies in LES and the mean velocity in RAS.) The difference is that in RAS,  $u'$  represents all the turbulent motions, while in LES,  $u'$  represents only the small eddies or subgrid scales. This means that the energy in the

unresolved scales of LES (subgrid scales) is a much smaller portion of the total flow compared to the energy in the unresolved scales of RAS (the turbulent fluctuations.) Hence, it is believed that the accuracy in the modelling of the SGS stress is not as crucial as the modelling of the Reynolds stress term in RAS.

It should be noted here that our treatment of the closure problem, Eqn. (8), is what Mason [18] refers to as the Lilly-Deardorff approach. This approach allows us to define the filtering operator implicitly through the modelling of the SGS stress term. Another approach, referred to as the Leonard approach, is to substitute

$$u_\alpha = \bar{u}_\alpha + u'_\alpha$$

into  $\overline{u_\alpha u_\beta}$  to get

$$\overline{u_\alpha u_\beta} = \overline{\bar{u}_\alpha \bar{u}_\beta} + \overline{u'_\alpha \bar{u}_\beta} + \overline{\bar{u}_\alpha u'_\beta} + \overline{u'_\alpha u'_\beta}.$$

Note that the first term on the right hand side of the above equation can be explicitly calculated if the filter used is itself explicitly defined. Using the above, the SGS stress term in Eqn. (8) becomes

$$\tau_{\alpha\beta} = (\overline{\bar{u}_\alpha \bar{u}_\beta} - \bar{u}_\alpha \bar{u}_\beta) + (\overline{u'_\alpha \bar{u}_\beta} + \overline{\bar{u}_\alpha u'_\beta}) + \overline{u'_\alpha u'_\beta}. \quad (9)$$

The advantage of the Leonard approach is that it breaks the SGS stress into three terms that have physical interpretations in the flow. The first term on the right hand side of Eqn. (9) represents the interaction of large eddies that produce small eddy effects and is called the Leonard stress. The second term, called the cross term, represents the interaction between the large and small eddies and the third term



represents the interaction of small eddies to produce large eddy effects. It is this term that produces the transfer of energy from the small to the large eddies and soe is known as the backscatter term. Note that the second term may also produce backscatter. The disadvantage of the Leonard approach is that the filter must be explicitly known for the calculation of the Leonard stress term. This may not be a trivial task, especially in grid base methods where the filter is often implicitly defined. As pointed out by Mason [18] and Ferziger [4], both the Lilly-Deardorff and Leonard approaches have been used successfully by researchers. The approach taken for our work is that of Lilly-Deardorff.

## 2.4 Subgrid Scale Models

As discussed in the previous section, in filtering the Navier–Stokes equations a new term is introduced which leads to a closure problem. To deal with this problem, the filtered Navier–Stokes equations are rewritten into the form given in Eqn. (8) and the new term,  $\tau_{\alpha\beta}$ , is then modelled. In this section, we will review two of the most commonly used SGS models, namely the Smagorinsky and the Dynamic Subgrid Scale models, and introduce our variant of the Smagorinsky model, which we will refer to as the Modified Smagorinsky model.

### 2.4.1 Smagorinsky Model

The Smagorinsky [25] subgrid scale model,

$$\tau_{\alpha\beta} - \frac{1}{3}\tau_{\gamma\gamma}\delta_{\alpha\beta} = -\nu_T \left( \frac{\partial \overline{u_\alpha}}{\partial x_\beta} + \frac{\partial \overline{u_\beta}}{\partial x_\alpha} \right) = -2\nu_T \overline{S}_{\alpha\beta} \quad (10)$$

where  $\nu_T$  is called the eddy viscosity (to be derived below) and

$$\overline{S}_{\alpha\beta} = \frac{1}{2} \left( \frac{\partial \overline{u_\alpha}}{\partial x_\beta} + \frac{\partial \overline{u_\beta}}{\partial x_\alpha} \right),$$

is known as an eddy viscosity type model because it assumes that the small eddies remove energy from the flow through a dissipative process. This precludes the possibility of backscatter (the reintroduction of energy from the small to large eddies) which is considered one of the model's weak points. The following derivation of the model is that of Ferziger [4].

According to turbulence theory, energy is introduced at the largest scales and is successively transferred to the smaller scales until viscous damping becomes the dominant effect. In the region where the viscous effect becomes dominant, the turbulent energy of the flow is damped out by the transfer of the kinetic energy to internal energy. Between these two scales is a region known as the inertial subrange, where there is neither significant production nor dissipation of energy. In this region, only the inviscid mechanisms are active and so assuming that the transfer of energy is always from the large to small scales, the term responsible for the transfer of this energy is then the advection term of the Navier–Stokes equations. This allows us to estimate the rate of energy transfer to the small scales as the magnitude of the contribution

of the advection term to the kinetic energy equation, which is

$$\frac{1}{2} \frac{\partial}{\partial x_\beta} (u_\alpha u_\alpha u_\beta).$$

Since energy is introduced at the largest scales, we estimate the dissipation rate,  $\epsilon$ , as

$$\epsilon \approx U_L^3/L \tag{11}$$

where  $U_L$  is the velocity scale of the large eddies and  $L$  is the integral length scale of the turbulent flow. Furthermore, if we assume that the largest subgrid scales are much larger than the viscous scales, then

$$\epsilon \approx U_{SGS}^3/\Delta \tag{12}$$

where  $U_{SGS}$  is the velocity scale of the small eddies and  $\Delta$  is the length of the largest subgrid scale eddies, which is also the length scale associated with the filter.

Now, as stated before, turbulence theory states that energy is transferred from the large to small scales. We assume that this process is dissipative in nature with respect to the large eddies (i. e. once the energy is lost by the large eddies to the small, it cannot be recovered.) So, the SGS model represents this energy transfer as effective viscous dissipation. Since it is the smallest resolved scales (of size  $\Delta$ ) that are most influenced by the SGS model, we estimate the effective dissipation as

$$\epsilon \approx \nu_T U_{SGS}^2/\Delta^2. \tag{13}$$

Using (12) and (13), we get

$$\nu_T \propto \Delta U_{SGS}$$

and using the above together with Eqns. (11) and (12)

$$\nu_T \approx \Delta^{\frac{4}{3}} L^{-\frac{1}{3}} U_L.$$

Using

$$U_L \approx L(2\overline{S}_{\alpha\beta}\overline{S}_{\alpha\beta})^{\frac{1}{2}} = L|\overline{S}|$$

we get

$$\nu_T = C_S^2 \Delta^{\frac{4}{3}} L^{\frac{2}{3}} |\overline{S}|$$

where  $C_S$  is the Smagorinsky parameter which is introduced to produce the equality.

Because of the difficulty in calculating the integral length scale,  $L$ , most researchers make the simplifying substitution

$$\Delta^{\frac{4}{3}} L^{\frac{2}{3}} \rightarrow \Delta^2$$

which leads to the more common form of the eddy viscosity in the Smagorinsky model,

$$\nu_T = (C_S \Delta)^2 |\overline{S}|. \quad (14)$$

In our calculations we use as our length scale

$$\Delta = (\Delta_1 \Delta_2 \Delta_3)^{\frac{1}{3}}$$

where  $\Delta_\alpha$  is the grid element length in the appropriate direction and set

$$C_S = 0.065.$$

Although the Smagorinsky model is the most widely recognized and used SGS model, it is not without its problems. One significant problem is that in non-homogeneous wall bounded flows, near the surface of the walls, the model does not

damp out the eddy viscosity enough to allow kinematic viscosity effects to become dominant. In fact, as the wall and hence the viscous sublayer is approached, our approximation, (12), in the derivation of the model itself becomes questionable since the grid points, hence  $\Delta$ , will be in or near the viscous sublayer region.

Another problem as mentioned before, is that since the Smagorinsky model assumes that the transfer of energy from large to small scales is a diffusive process, Eqn. (13), no mechanism exists to transfer energy from the small to the large scales, i. e. there is no backscatter. To show this, we follow the work of Piomelli *et al.* [22] and observe that in the resolved energy transport equation,

$$\frac{\partial \bar{q}^2}{\partial t} + \frac{\partial(\bar{q}^2 \bar{u}_\beta)}{\partial x_\beta} = \frac{\partial}{\partial x_\beta} \left( -2\bar{p} \bar{u}_\beta - 2\bar{u}_\alpha \tau_{\alpha\beta} + \frac{1}{Re} \frac{\partial \bar{q}^2}{\partial x_\beta} \right) - \frac{2}{Re} \frac{\partial \bar{u}_\alpha}{\partial x_\beta} \frac{\partial \bar{u}_\alpha}{\partial x_\beta} + 2\tau_{\alpha\beta} \bar{S}_{\alpha\beta}.$$

where  $\bar{q}^2 = \bar{u}_\alpha \bar{u}_\alpha$ , one-half of the last term,

$$\epsilon_{SGS} = \tau_{\alpha\beta} \bar{S}_{\alpha\beta}$$

which is referred to as the “subgrid-scale dissipation”, represents the transfer of energy between the large and small scales. Note that

$$\epsilon_{SGS} < 0$$

indicates that the resolved energy decays with respect to the interaction between the large and small scales (forward scatter), while

$$\epsilon_{SGS} > 0$$

means that the resolved energy grows with respect to the interaction of the large and small scales (backscatter). In the case of the Smagorinsky model, Equations

(10) and (14) clearly show that  $\epsilon_{SGS} < 0$ , and so there is no backscatter when the Smagorinsky model is used. In their study using DNS data, Piomelli *et al.* [22] found that for channel flow using a Sharp-Cutoff filter, nearly 50% of the points experienced backscatter. For the Gaussian filter, the percentage dropped to about 30% and the Top-Hat filter fell inbetween the cutoff and the Gaussian. These results indicate that although in the mean, the net effect of the SGS dissipation is forward scatter, there is significant backscatter. The importance of backscatter in the SGS model is not yet clear. In fully developed channel flows for example, purely dissipative SGS stress models have been used successfully. Since forward scatter is dominant in the mean, this would seem reasonable. As Piomelli *et al.* [22] speculated, it would seem reasonable that backscatter effects would be more important for nonequilibrium flows.

Finally, there is the problem of setting the Smagorinsky parameter,  $C_S$ . The values used range from about 0.2 for isotropic turbulence to 0.065 for the channel flow. Other than for isotropic turbulence, the author is not aware of any systematic analysis to determine the parameter.

#### 2.4.2 Dynamic Subgrid Scale Model

To overcome the problems of the Smagorinsky model, Germano *et al.* [6] introduced a method of calculating the Smagorinsky parameter interactively during run time rather than setting the parameter to a fixed constant at the beginning of the numerical calculations. Here, we introduce a variant of Germano's dynamic procedure developed

by Piomelli and Liu [23]. The procedure involves applying a second filter, which is called the test filter  $\tilde{\cdot}$ , to the filtered momentum equation, Eqn. (7). This results in

$$\frac{\partial \tilde{\tilde{u}}_\alpha}{\partial t} + \frac{\partial}{\partial x_\beta} (\tilde{\tilde{u}}_\alpha \tilde{\tilde{u}}_\beta) = -\frac{\partial \tilde{\tilde{P}}}{\partial x_\alpha} - \frac{\partial \mathcal{T}_{\alpha\beta}}{\partial x_\beta} + \frac{1}{Re} \frac{\partial^2}{\partial x_\beta^2} \tilde{\tilde{u}}_\alpha$$

where

$$\mathcal{T}_{\alpha\beta} = \overline{\tilde{u}_\alpha \tilde{u}_\beta} - \tilde{u}_\alpha \tilde{u}_\beta.$$

Now we define the resolved turbulent stress as

$$\mathcal{L}_{\alpha\beta} = \overline{\tilde{u}_\alpha \tilde{u}_\beta} - \tilde{u}_\alpha \tilde{u}_\beta$$

which represents the contribution of the small resolved scales to the Reynolds stresses.

Using the Smagorinsky model as our SGS model, we have at the filter and test filter level,

$$\tau_{\alpha\beta} - \frac{1}{3} \tau_{\gamma\gamma} \delta_{\alpha\beta} \approx -2C_S \Delta^2 |\overline{S}| \overline{S}_{\alpha\beta} = -2C_S B_{\alpha\beta} \quad (15)$$

$$\mathcal{T}_{\alpha\beta} - \frac{1}{3} \mathcal{T}_{\gamma\gamma} \delta_{\alpha\beta} \approx -2C_S \tilde{\Delta}^2 |\tilde{S}| \tilde{S}_{\alpha\beta} = -2C_S A_{\alpha\beta} \quad (16)$$

where we have used  $C_S$  rather than  $C_S^2$  in the eddy viscosity term, Eqn. (14), and  $\Delta$  and  $\tilde{\Delta}$  represents the width of the first filter and the test filter, respectively. Now, the SGS stresses at the filter and test filter level are related to the resolved turbulent stress through an algebraic identity known as Germano's identity,

$$\mathcal{L}_{\alpha\beta} = \mathcal{T}_{\alpha\beta} - \tilde{\tau}_{\alpha\beta}.$$

Note that if we use the models for the stresses, Eqns. (15) and (16), then Germano's identity is no longer satisfied exactly. Hence, we obtain the residual equation

$$E_{\alpha\beta} = \mathcal{L}_{\alpha\beta} + 2C_S A_{\alpha\beta} - 2C_S \tilde{B}_{\alpha\beta}. \quad (17)$$

Piomelli's method is to minimize the square of the residual assuming that the Smagorinsky parameter,  $C_S$ , is known (denoted by  $C_S^*$ ) in the third term on the right side of Eqn. (17). So the residual equation becomes

$$E_{\alpha\beta} = \mathcal{L}_{\alpha\beta} + 2C_S A_{\alpha\beta} - 2C_S^* \widetilde{B}_{\alpha\beta}$$

and minimizing the square of the residual yields

$$C_S = -\frac{1}{2} \frac{(\mathcal{L}_{\alpha\beta} - 2C_S^* \widetilde{B}_{\alpha\beta}) A_{\alpha\beta}}{A_{\xi\eta} A_{\xi\eta}}. \quad (18)$$

The Smagorinsky parameter,  $C_S^*$  is then approximated using a Taylor series expansion of  $C_S$ .

One of the advantages of the DSGS model is that there are no parameters to determine before the numerical run. Also, the DSGS model is able to reduce the eddy viscosity in the laminar regions of the flow. Finally, the DSGS model can allow for backscatter in the flow.

Although Piomelli's version of the DSGS model was formulated to answer some of the problems with Germano's original dynamic procedure, there are still some unresolved issues with the model. One of the problems is that in the derivation of the model, the Smagorinsky parameter was assumed to be independent of the filter width (see Eqns. (15) and (16).) However, using DNS data from isotropic turbulence, Meneveau [20] found that the instantaneous values of the Smagorinsky parameter varied significantly when computed at two different filter widths.

Another problem with the DSGS model is that, as formulated, it allows  $C_S$  and hence the eddy viscosity to be negative. Although this allows the model to account



for backscatter, if the eddy viscosity remains negative long enough, it can lead to numerical instabilities. Researchers have found this to be case and some type of an artificial constraint is usually required to prevent this instability. In our case, we use the constraint

$$C_S \geq C_{min}$$

where  $C_{min} = -0.01$ .

Also, during the execution of the DSGS model, it was found that if we calculate  $C_S$  at each time step, then Eqn. (18) can and does become unstable. So, to stabilize the calculations, we use time averaged values to calculate  $C_S$ . The time interval used is kept small (100 time steps) to preserve the dynamic nature of the model in time as well as in space.

Finally, although not so much a problem as it is a question, is the issue of the double filtering. In the derivation of the DSGS model, it is assumed that filtering twice is equivalent to filtering once with some filter. This assumption is used to apply the Smagorinsky SGS model to the SGS stress term at the test filter level, Eqn. (16). In Appendix B, we derive explicitly the filters that are equivalent to filtering twice with the Gaussian and the Top-Hat filter.

### 2.4.3 Modified Smagorinsky Model

One of the problems of the Smagorinsky model as mentioned above, is that the eddy viscosity does not damp out as the walls are approached. To overcome this problem

we introduce a damping function in the calculation of the Smagorinsky parameter. The damping function is constructed under the constraint that the distance from the wall cannot be used directly by the model and that the new model cannot significantly increase resource usage (e. g. cpu time and memory.)

To construct our damping function, we first define the instantaneous kinetic energy as

$$\kappa = \frac{1}{2} \bar{u}_\alpha \bar{u}_\alpha,$$

the instantaneous dissipation rate as

$$\epsilon = \nu \frac{\partial \bar{u}_\alpha}{\partial x_\beta} \frac{\partial \bar{u}_\alpha}{\partial x_\beta},$$

and the instantaneous Reynolds number as

$$Re_{inst} = \frac{\kappa^2}{\nu \epsilon}.$$

Note that near the wall, if we Taylor expand  $\bar{u}_\alpha$  assuming that the wall location is at  $\mathbf{x} = 0$ , then the only non-zero derivative of the velocity vector will be in the wall normal direction,  $y$ , assuming the wall to be in the x-z plane. So

$$\bar{u}_\alpha = \bar{u}_\alpha \Big|_{\mathbf{x}=0} + y \frac{\partial \bar{u}_\alpha}{\partial y} \Big|_{\mathbf{x}=0} + \dots$$

By the no slip boundary condition,  $\bar{u}_\alpha(\mathbf{0}) = 0$ , and so

$$O(\kappa) = y^2.$$

Using a similar argument, we have that

$$O(\epsilon) = 1.$$

So

$$Re_{inst} \sim y^4.$$

Hence we use the instantaneous Reynolds number,  $Re_{inst}$ , to detect the wall. Since the Smagorinsky model works well away from the walls, our modified Smagorinsky model is

$$\nu_T = (C'_S \Delta)^2 |\bar{S}| \quad (19)$$

where

$$C'_S = C_S \begin{cases} \left(\frac{Re_{inst}}{Re^o}\right)^\gamma & \text{for } 0 \leq Re_{inst} \leq Re^o \\ 1 & \text{for } Re_{inst} > Re^o \end{cases}$$

and

$$Re^o = \mu [Re_{inst}]_{max}.$$

Note that  $\gamma$  and  $\mu$  are just model parameters and that  $[Re_{inst}]_{max}$  represents the largest value of  $Re_{inst}$  in the computational domain at a given instant in time.

As will be shown in the results section, our model is able to detect the walls and damp out the eddy viscosity. However, there is nothing in the derivation of the model that indicates that  $Re_{inst} \leq Re^o$  only near the wall surfaces. In fact, as will be seen in the results for the channel and backward facing step problems,  $Re_{inst} \leq Re^o$  occurs quite often in elements far from the walls.

### 3 Channel Flow

We use the channel flow as a benchmark to test the three subgrid scale models, because of the extensive amount of data, both experimental and theoretical, that is available for this type of flow. Since fully developed turbulent channel flow is homogeneous in both the streamwise and spanwise directions, we use periodic boundary conditions in those directions.

#### 3.1 Computational Parameters

The computational domain of the channel consists of  $53 \times 32 \times 16$  elements and its dimensions are  $10h$  in the streamwise direction ( $x$ ),  $2h$  in the spanwise direction ( $z$ ) and  $2h$  in the wall normal direction ( $y$ ), where  $h$  ( $= 0.5$ ) is the channel half height. A sketch of the channel is given in Fig. 1.

For initial data, we use the following:

$$\begin{cases} u = f(y) + \epsilon u^* \\ v = \epsilon v^* \\ w = \epsilon w^*, \end{cases}$$

where  $f(y)$  is a parabolic function zero at the walls and one at the channel center,  $\epsilon = 0.1$ , and  $u^*$ ,  $v^*$ , and  $w^* \in [-1, 1]$  (uniform distribution.) In our flow experiments, we set the viscosity,  $\nu = 10^{-4}$ . So, using mean initial streamwise center line velocity,  $U_0 = 1$  as our velocity scale, and the channel height,  $2h = 1$ , as our integral length

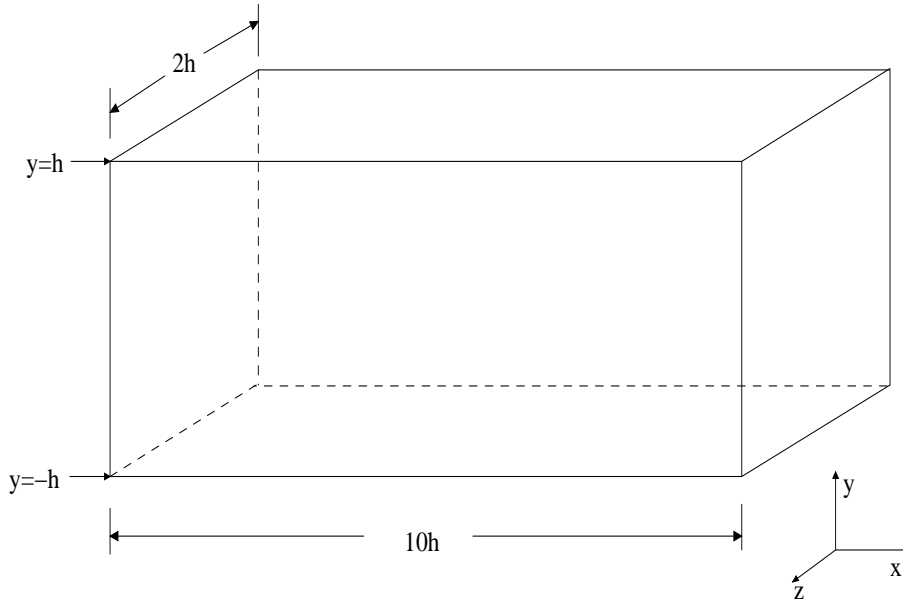


Figure 1: *Sketch of the channel with relevant dimensions. For our experiment, we use  $h = 0.5$*

scale, we estimate the Kolmogorov length scale as

$$\eta \approx \left( \frac{2hU_0}{\nu} \right)^{-\frac{3}{4}} = (Re_0)^{-\frac{3}{4}} = 0.001.$$

Hence, near the walls, we grade the grid so that the smallest element will have a height of  $O(10^{-3})$ . A sketch of the graded grid in the  $xy$ -plane face of the channel is shown in Fig. 2. Note that the grading in the streamwise direction was done to reduce the number of grid points needed in the streamwise direction. It is not a result of any physics of the flow, as in the wall normal direction. A uniform grid is used in the spanwise direction.

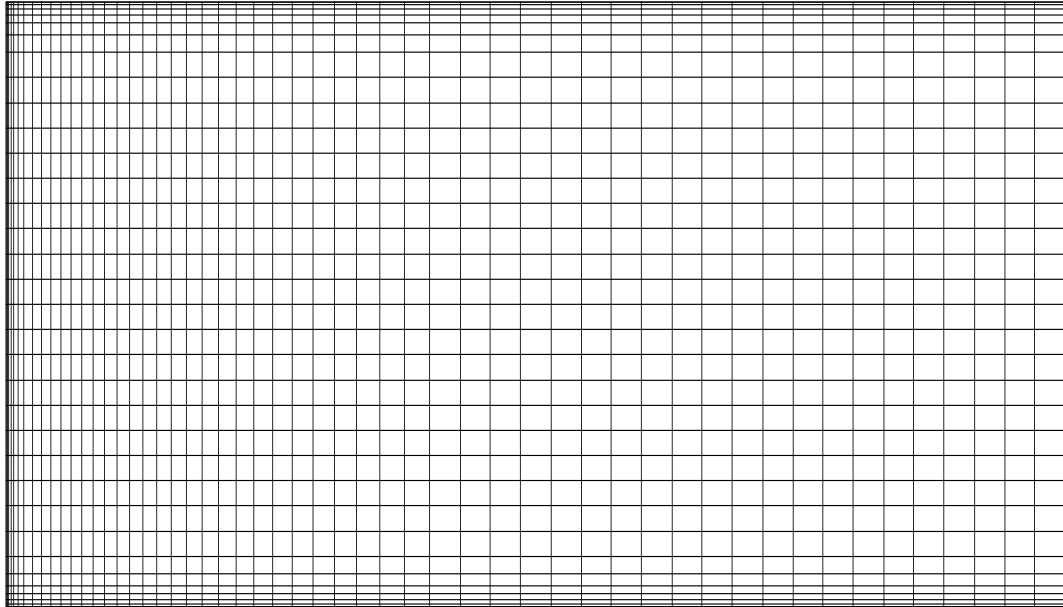


Figure 2: *Sketch of the  $xy$ -plane face of the graded channel grid.*

### 3.2 Constant Flow Rate

In assuming periodic boundary conditions in the streamwise direction, the computational grid is in essence following the flow down stream. In order to maintain a time dependent flow, an external force must be applied to the flow. In the case of the channel, a negative streamwise pressure gradient is used to sustain the flow. To calculate this pressure gradient, we follow the procedure described by Tran and Morchoisne [27] in which the pressure gradient is found in such a way that the flow rate remains constant. Let

$$F_\alpha = (F_x(t), 0, 0)$$

be the streamwise pressure gradient which may vary in time but is constant in space. Using the centerline velocity,  $U_0$ , and channel half height,  $h$ , as our characteristic velocity and length, the non-dimensionalized momentum equations are

$$\frac{\partial U_\alpha}{\partial t} + \frac{\partial}{\partial x_\beta}(U_\alpha U_\beta) = -\frac{\partial P}{\partial x_\alpha} + \frac{1}{Re_0} \frac{\partial^2 U_\alpha}{\partial x_\beta \partial x_\beta} + F_\alpha, \quad (20)$$

where  $Re_0 = \frac{U_0 h}{\nu}$ .

Since the flow is assumed to be homogenous in the stream and spanwise directions, we define our averaging operator to be

$$\langle f \rangle_{x,z}(y) = \frac{1}{L_x L_z} \int_0^{L_x} \int_0^{L_z} f(x, y, z) dx dz, \quad (21)$$

where  $L_x$  and  $L_z$  are the streamwise and spanwise lengths of the channel, and the mean flow rate as

$$Q = \frac{L_z}{h} \int_{-1}^1 \langle U \rangle_{x,z} dy. \quad (22)$$

So, integrating the streamwise momentum equation, Eqn. (20), we get

$$\frac{L_z}{h} \frac{1}{L_x L_z} \int_{-1}^1 \int_0^{L_z} \int_0^{L_x} \left\{ \underbrace{\frac{\partial U}{\partial t}}_A + \underbrace{\frac{\partial}{\partial x_\beta}(UU_\beta)}_B = \underbrace{-\frac{\partial P}{\partial x}}_C + \underbrace{\frac{1}{Re_0} \frac{\partial^2 U}{\partial x_\beta \partial x_\beta}}_D + \underbrace{F_x}_E \right\} d\mathbf{x}. \quad (23)$$

We simplify each term in the above equation as follows:

- Using Eqn. (21) and (22), A is simply  $\frac{\partial Q}{\partial t}$ .
- For term B, we break up the sum and simplify each term separately. The first term is

$$\int_{-1}^1 \int_0^{L_z} \int_0^{L_x} \frac{\partial}{\partial x}(U^2) d\mathbf{x} = \int_{-1}^1 \int_0^{L_z} U^2 \Big|_{x=0}^{x=L_x} = 0$$

since the flow is periodic in the  $x$  direction. Similarly, since the flow is also periodic in the  $z$  direction, we have that

$$\int_{-1}^1 \int_0^{L_z} \int_0^{L_x} \frac{\partial}{\partial z}(UW) d\mathbf{x} = 0.$$

For the third term,

$$\int_{-1}^1 \int_0^{L_z} \int_0^{L_x} \frac{\partial}{\partial x}(UV) d\mathbf{x} = \int_0^{L_x} \int_0^{L_z} UV \Big|_{y=-1}^{y=1} = 0$$

by the no-slip boundary condition along the walls. So,  $B = 0$ .

- $C$  must also be zero, for if the mean pressure gradient was not zero, then there would be no need to add an external force,  $F_x$ , to drive the flow.
- For  $D$ , we break up the sum as we did for  $B$ . So

$$\int_{-1}^1 \int_0^{L_z} \int_0^{L_x} \frac{\partial^2 U}{\partial x^2} = \int_{-1}^1 \int_0^{L_z} \frac{\partial U}{\partial x} \Big|_{x=0}^{x=L_x} = 0$$

since the flow is periodic in the  $x$  direction. A similar argument can be used to show that

$$\int_{-1}^1 \int_0^{L_z} \int_0^{L_x} \frac{\partial^2 U}{\partial z^2} = 0.$$

For the third term, we have that

$$\begin{aligned} \frac{L_z}{h} \frac{1}{L_x L_z} \int_{-1}^1 \int_0^{L_z} \int_0^{L_x} \frac{1}{Re_0} \frac{\partial^2 U}{\partial y^2} &= \frac{L_z}{h} \frac{1}{Re_0} \int_{-1}^1 \frac{\partial^2 \langle U \rangle_{x,z}}{\partial y^2} dy \\ &= \frac{L_z}{h} \frac{1}{Re_0} \frac{\partial \langle U \rangle_{x,z}}{\partial y} \Big|_{y=-1}^{y=1}. \end{aligned}$$

Since the mean channel flow is symmetric about the channel center line,  $y = 0$ ,

$$\frac{\partial \langle U \rangle_{x,z}}{\partial y} \Big|_{y=1} = - \frac{\partial \langle U \rangle_{x,z}}{\partial y} \Big|_{y=-1}.$$



So,

$$D = \frac{L_z}{h} \frac{1}{Re_0} \frac{\partial \langle U \rangle_{x,z}}{\partial y} \Big|_{y=-1}^{y=1} = -2 \frac{L_z}{h} \frac{1}{Re_0} \frac{\partial \langle U \rangle_{x,z}}{\partial y} \Big|_{y=-1}.$$

- Finally, since  $F_x$  is constant in space, E simplifies to

$$\frac{L_z}{h} \frac{1}{L_x L_z} \int_{-1}^1 \int_0^{L_z} \int_0^{L_x} F_x d\mathbf{x} = \frac{2L_z}{h} F_x.$$

Using the above, Eqn. (23) can be rewritten as

$$\frac{\partial Q}{\partial t} = -2 \frac{L_z}{h} (u_\tau^2 - F_x), \quad (24)$$

where  $u_\tau^2 = \frac{1}{Re_0} \frac{\partial \langle U \rangle_{x,z}}{\partial y} \Big|_{y=-1}$  is the mean wall shear stress. So, as the flow changes from a laminar state to a turbulent state,  $u_\tau^2$  increases and if the pressure gradient is kept constant at the laminar value, Eqn. (24) says that  $Q$  will decrease. To maintain a constant flow rate,  $Q$ , it is then necessary to balance the pressure gradient to the mean wall shear stress. However, to calculate the mean wall shear stress would require a large grid to obtain the mean values in the stream and spanwise directions. This makes balancing the pressure gradient with the mean wall shear stress computationally too expensive. So,  $F_x$  is found by relating the pressure gradient to the flow rate fluctuations from the constant initial value  $Q_0$ ,

$$F^{n+1} = F^n - a_1(Q^{n+1} - Q_0) - a_2(Q^n - Q_0)$$

where  $a_1 = 2\Delta t$ ,  $a_2 = \Delta t$ , and  $n$  and  $n + 1$  represent the old and new time states.

Note that the formula given in the reference, [27], contains typographical errors.

### 3.3 Numerical Results

Using the mean initial centerline velocity as our characteristic velocity and the channel half height as our characteristic length scale, the Reynolds number for our numerical experiments is  $Re_C^0 = 5000$ . Note that in the following discussion that all mean calculations are based on averaging in the homogeneous directions (x and z) as well as time. Also, note that we use as our characteristic velocity for non-dimensionalization, the wall shear velocity

$$u_\tau = \left( \frac{\tau_w}{\rho} \right)^{\frac{1}{2}}$$

where  $\tau_w$  is the wall shear stress and use as our non-dimensional wall distance

$$y^+ = \frac{yu_\tau}{\nu}.$$

Fig. 3 is a plot of the total kinetic energy using the three different models. As can be seen in the figure, by simulation time  $t = 150$ , the flow has stabilized enough to begin the time averaging calculations. Note that in the DSGS model run, the Smagorinsky model is used while the flow is developing until time  $t = 75$ . This is the reason for the initial overlap of energy between the Smagorinsky and DSGS results in Fig. 3.

One of the problems with the Smagorinsky model discussed above is that the eddy viscosity is not damped as the wall and the viscous sublayer is approached. This can clearly be seen in Fig. 4, the sketch of the time averaged eddy viscosity along the lines  $x = 5h$  and  $z = 1.0625h$ , and  $x = 9h$  and  $z = 1.0625h$ . Note that along these lines,

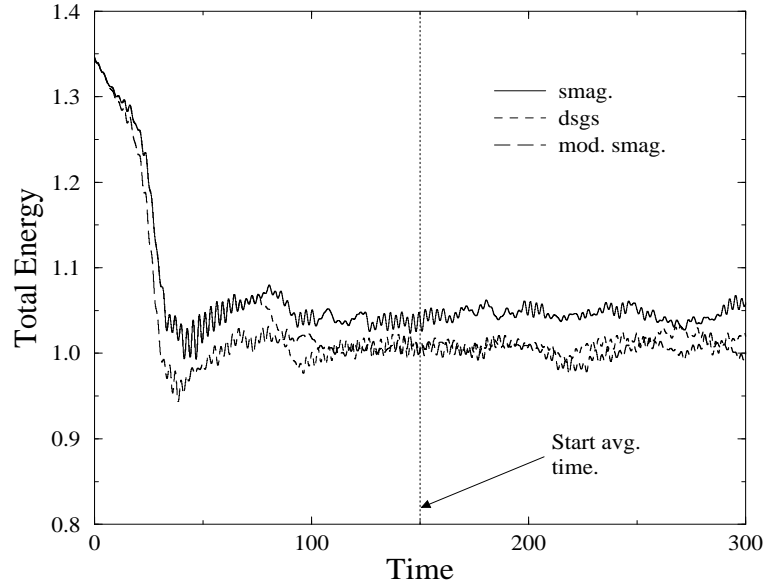


Figure 3: *Plot of the total kinetic energy for the channel flow using the Smagorinsky, DSGS, and modified Smagorinsky subgrid scale models. At time  $t = 150$ , a running total of the fluid variables are started to calculate the various mean properties of the flow.*

the magnitude of the eddy viscosity is approximately 75% of the kinematic viscosity at the walls, when using the Smagorinsky model. The plots also show that both the DSGS and the modified Smagorinsky model damp out the eddy viscosity as the wall is approached. Fig. 4 also indicates that the damping function in the modified Smagorinsky model not only damps out the eddy viscosity near the walls but also causes some damping far from the walls. However, the plots show that the damping along the central region of the channel is not as great as the damping near the walls. Fig. 5, a snap shot of the eddy viscosity along the line  $x = 5h$  and  $z = 1.0625h$  at simulation times  $t = 150$  and  $t = 300$ , shows that at any given time, the eddy viscosity

can be over a magnitude greater than the kinematic viscosity when using the DSGS model. Furthermore, Fig. 5b shows that at any given time, the eddy viscosity can be negative (which can be interpreted as backscatter) when using the DSGS model.

Fig. 6, a log-linear plot of the non-dimensionalized mean velocity, indicates that the modified Smagorinsky data is much closer to the logarithmic friction law than the Smagorinsky model. Note that we use as our additive constant in the log law, 5.5, as in Kim, Moin, and Moser's work [12] since our Reynolds number, based on the wall shear velocity, is  $Re_\tau \approx 180$  for our channel computations.

Figures 7 – 9 are plots of the root-mean-square of the velocity fluctuations. Note that the DNS results to which we compare our data is that of Kim et al. [12] and the experimental data is that of Kreplin and Eckelmann [13]. It is not very surprising that the velocity fluctuation properties of our LES computations do not match the DNS and experimental results exactly, because of the way in which the fluctuations are computed. If we let  $\langle \cdot \rangle_{t,x,z}$  be the average in time and the homogeneous directions and  $'$  denotes the statistical fluctuations with zero mean, then note that

$$(u'_\alpha)^2 = \langle u_\alpha \rangle_{t,x,z}^2 - \langle u_\alpha^2 \rangle .$$

However, for our LES cases, the only values we have are at the filter level,  $\bar{u}_\alpha$ . Hence the only fluctuation we can calculate is

$$(\bar{u}'_\alpha)^2 = \langle \bar{u}_\alpha \rangle_{t,x,z}^2 - \langle \bar{u}_\alpha^2 \rangle_{t,x,z}$$

where  $\bar{u}'_\alpha$  represents the statistical fluctuations in the filtered field. Note that  $\bar{u}'_\alpha$  is well defined (in the sense that it will not be identically zero) since, as discussed in the

filter section, only the Sharp-Cutoff filter has compact support in wave space and so for filters such as the Top-Hat filter,  $\bar{u}_\alpha$  will still contain some small scale motions. Also, the grading of the grid near the walls implies that the filter width decreases near the walls and so will contain more of the small scale motions. Hence, we would expect  $\bar{u}'_\alpha$  to be closer to  $u'_\alpha$  near the walls, were the filter width is much smaller than toward the channel center. Figures 7 – 9 show that this is indeed the case.

Fig. 10 is a plot of the Reynolds shear stress normalized by the wall shear velocity. As discussed above, we note that the LES results are much closer to the DNS results near the wall. Also note that the DSGS and modified Smagorinsky are closer to the DNS results than using standard Smagorinsky model.

Figures 11 – 13 are plots of the root-mean-square vorticity fluctuations normalized by the mean wall shear. Since vorticity is mostly associated with small scale motions, it is not surprising that the LES vorticity data are all lower than the DNS data for the reason given above. Note that near the wall, at least one of the LES data is close to the DNS results. Unfortunately, there is no consistency as to which model is closest to the DNS results. For x vorticity fluctuations, the Smagorinsky model is closest to the DNS results near the wall, the modified Smagorinsky is the furthest off from the DNS data, and the DSGS model is between the other two. However, for the z vorticity, note that the order of performance of the models changes to the DSGS being the closest, followed by the modified Smagorinsky and then the Smagorinsky.

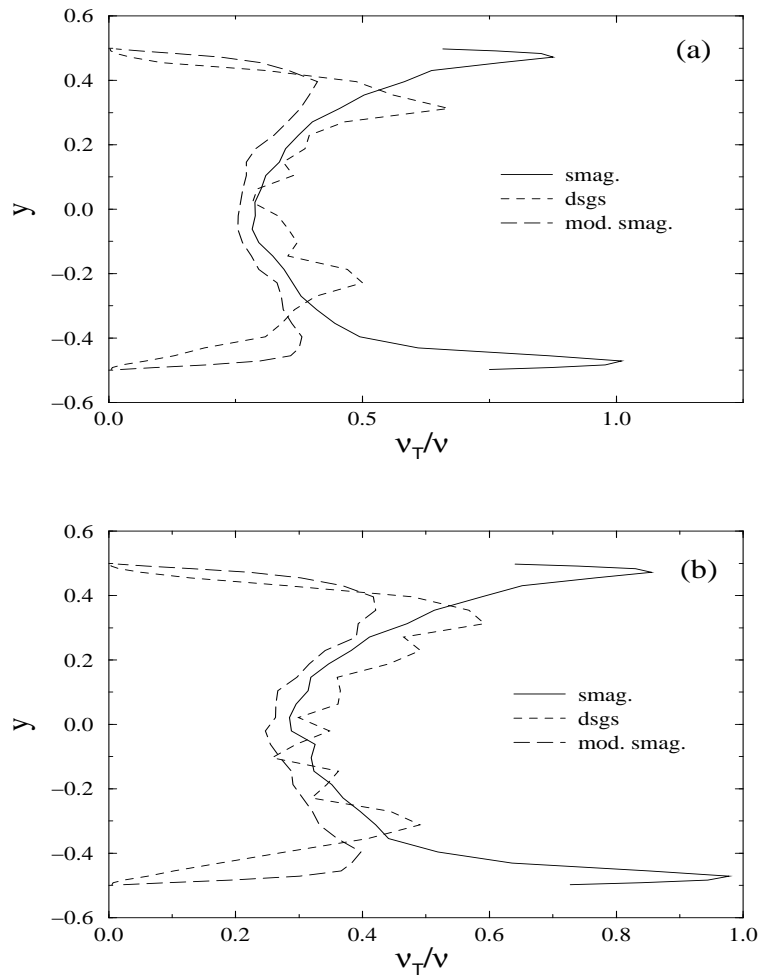


Figure 4: *Time averaged plots of the eddy viscosity normalized by the kinematic viscosity. (a) is a plot along the line  $x = 5h$  and  $z = 1.0625h$ . (b) is a plot along the line  $x = 9h$  and  $z = 1.0625h$ .*

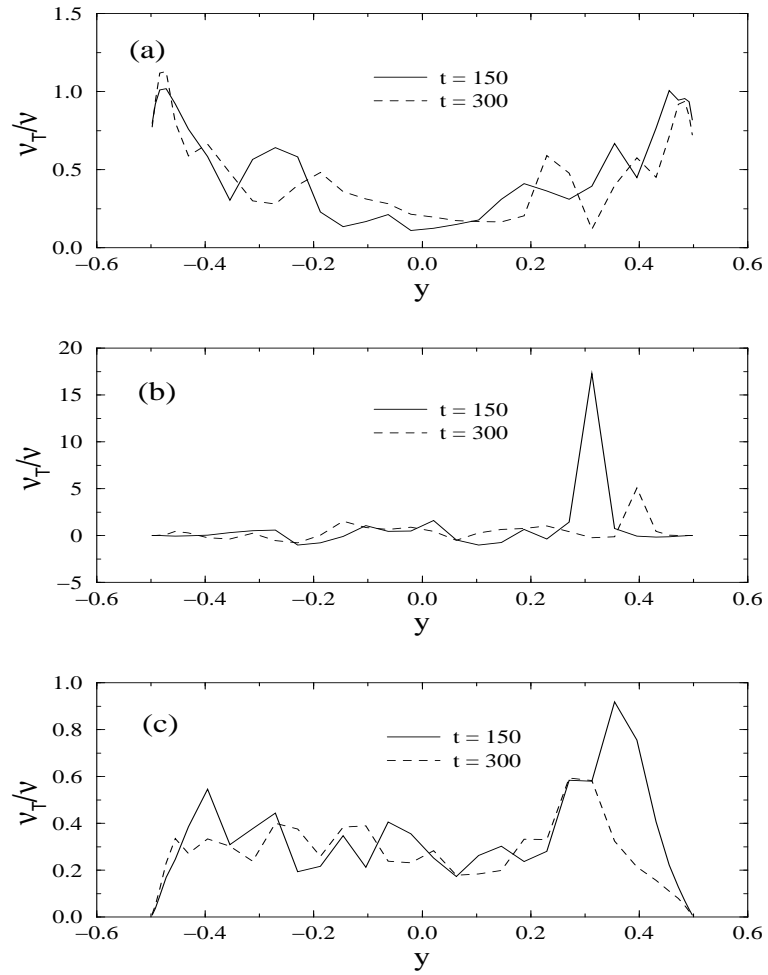


Figure 5: *Instantaneous snap shot of the eddy viscosity normalized by the kinematic viscosity along the line  $x = 5h$  and  $z = 1.0625h$ . (a) is using the Smagorinsky model, (b) is the DSGS model, and (c) is the modified Smagorinsky model.*

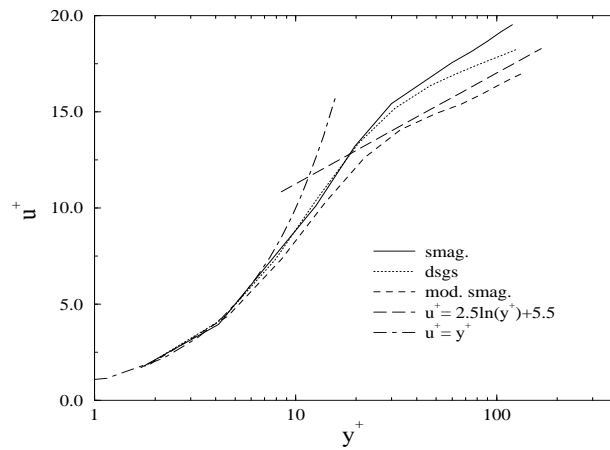


Figure 6: *Log-linear plot of the mean velocity normalized by the wall shear velocity,  $u_\tau$ , for the channel flow using the Smagorinsky, DSGS, and modified Smagorinsky subgrid scale models.*

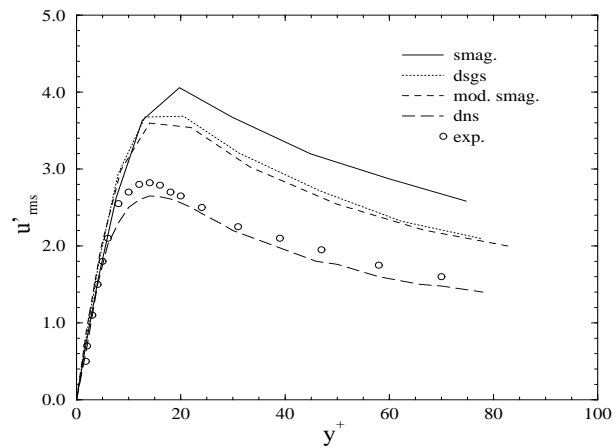


Figure 7: *Root-mean-square of the streamwise velocity fluctuations normalized by the wall shear velocity. Note that dns data is from Kim et al. [12] and the experimental data, exp, is from Kreplin and Eckelmann [13].*



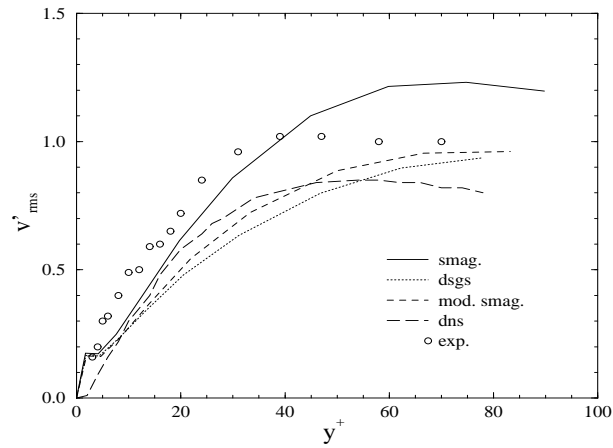


Figure 8: *Root-mean-square of the wall normal velocity fluctuations normalized by the wall shear velocity. Note that dns data is from Kim et al. [12] and the experimental data, exp, is from Kreplin and Eckelmann [13].*

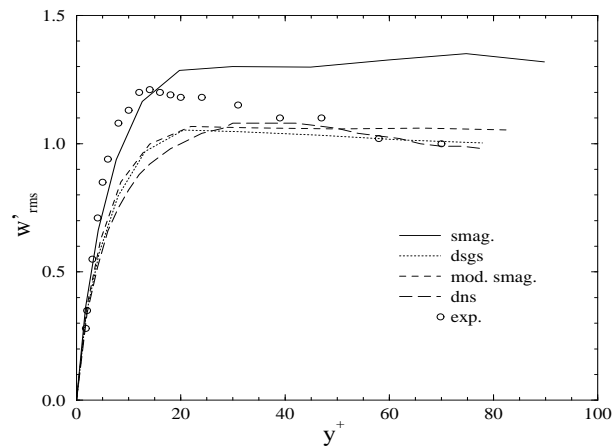


Figure 9: *Root-mean-square of the spanwise velocity fluctuations normalized by the wall shear velocity. Note that dns data is from Kim et al. [12] and the experimental data, exp, is from Kreplin and Eckelmann [13].*

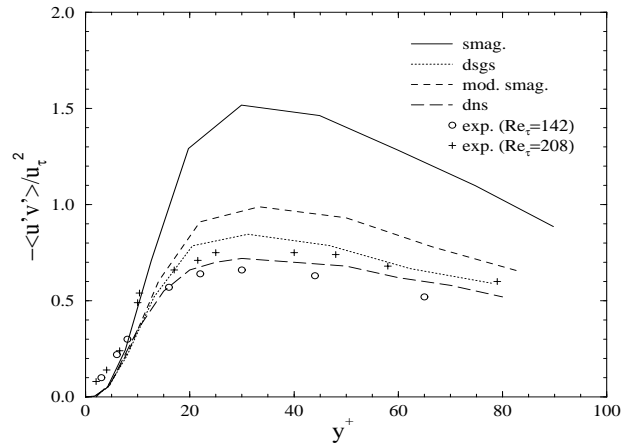


Figure 10: Reynolds shear stress normalized by the wall shear velocity. Note that dns data is from Kim et al. [12] and the experimental data, exp, is from Eckelmann [3] at two different Reynolds numbers,  $Re_\tau = 142$  and  $Re_\tau = 208$ .

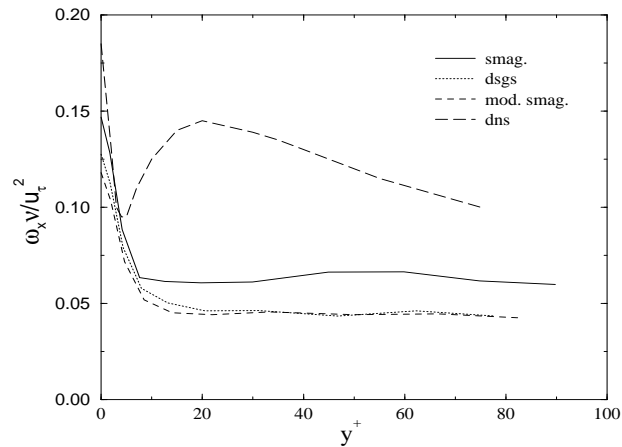


Figure 11: Root-mean-square vorticity ( $x$ ) fluctuations normalized by the mean wall shear. Note that dns data is from Kim et al. [12].

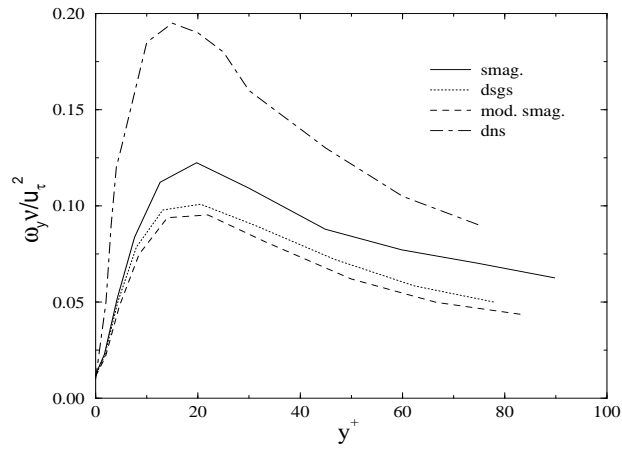


Figure 12: *Root-mean-square vorticity ( $y$ ) fluctuations normalized by the mean wall shear. Note that dns data is from Kim et al. [12].*

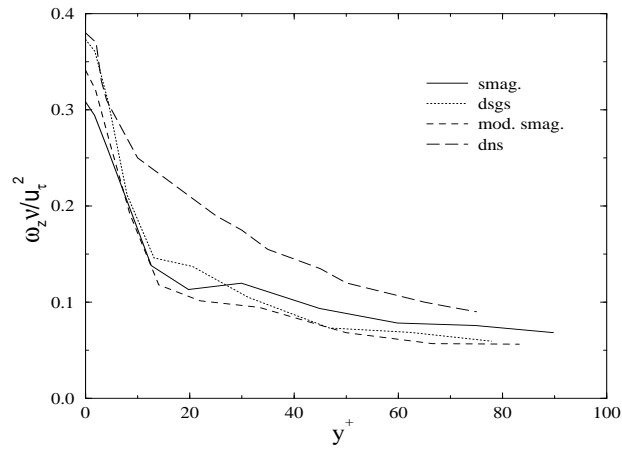


Figure 13: *Root-mean-square vorticity ( $z$ ) fluctuations normalized by the mean wall shear. Note that dns data is from Kim et al. [12].*

## 4 Flow over a Backward Facing Step

To study the effectiveness of the various SGS models on turbulent flows with separation and reattachment, the flow over a backward facing step is used because of its geometric simplicity. In our modeling of this flow, we use periodic boundary conditions in the spanwise direction.

### 4.1 Computational Parameters

The computational domain of our backward facing step problem consists of one main channel (post expansion section) with the step located at one end of the channel, see Fig. 14. The discretization of the channel consists of  $88 \times 32 \times 16$  elements and the dimensions of the channel are approximately  $20h$  in the streamwise direction and  $2h$  in the spanwise and wall normal directions, where  $h = 0.45833$  is the step height.

At the inlet, the fluid is forced by setting the streamwise velocity to be 1 along the inlet plane. Thus the Reynolds number, based on the inlet velocity and the step height, is  $Re_h = 4583$ .

### 4.2 Numerical Results

As in the channel flow simulations, the time averaging calculations are started once the total kinetic energy has reached a quasi-equilibrium state, see Fig. 15. Figure 16

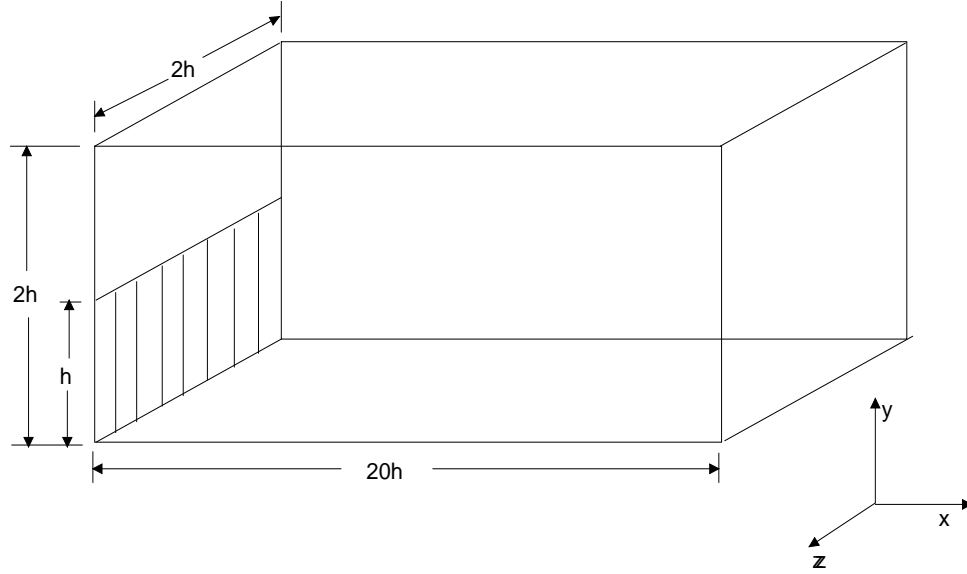


Figure 14: *Sketch of the backward facing step and channel with approximate relevant dimensions. For our experiment, the step height is  $h = 0.45833$*

is a plot of the mean skin friction coefficient,

$$C_f = \frac{\tau_w}{\frac{1}{2}\rho U_0^2}$$

along the bottom wall, where  $U_0$  is the inlet velocity. According to Le & Moin [15], the high  $|C_f|$  in the recirculation region is the result of not having an entry section.

Figures 17 and 18 are comparisons of the mean streamwise velocity at various locations in the recirculation, reattachment, and recovery regions. In the reattachment and recovery regions, the data indicate that near the wall all the LES models overpredicted the mean streamwise velocity. In the region of the secondary bubble, the skin friction data (Fig. 16) and the mean velocity data (Fig. 17) indicate that for the Smagorinsky model and the modified Smagorinsky model, the secondary bubble

is not as well defined as in the DNS and DSGS cases.

Figures 19–22 are the profiles of the various Reynolds stress components. Figure 19 indicates that in the reattachment region, all the SGS models predicted a greater streamwise turbulence intensity near the wall than the DNS results. According to Le and Moin [15], their results were lower than the experimental data of Jovic and Driver [11]. Also, the data from Akselvoll and Moin [1], indicate that their LES also predicted higher turbulence intensities, although not as high as our results. In the recirculation region, Le and Moin [15] reported that the maximum of all Reynolds stress components occurred around the step height. As can be seen in Figures 19–22, the maximum of all Reynolds stress components in the LES cases occur before the step height and does not peak as sharply as in the DNS case.

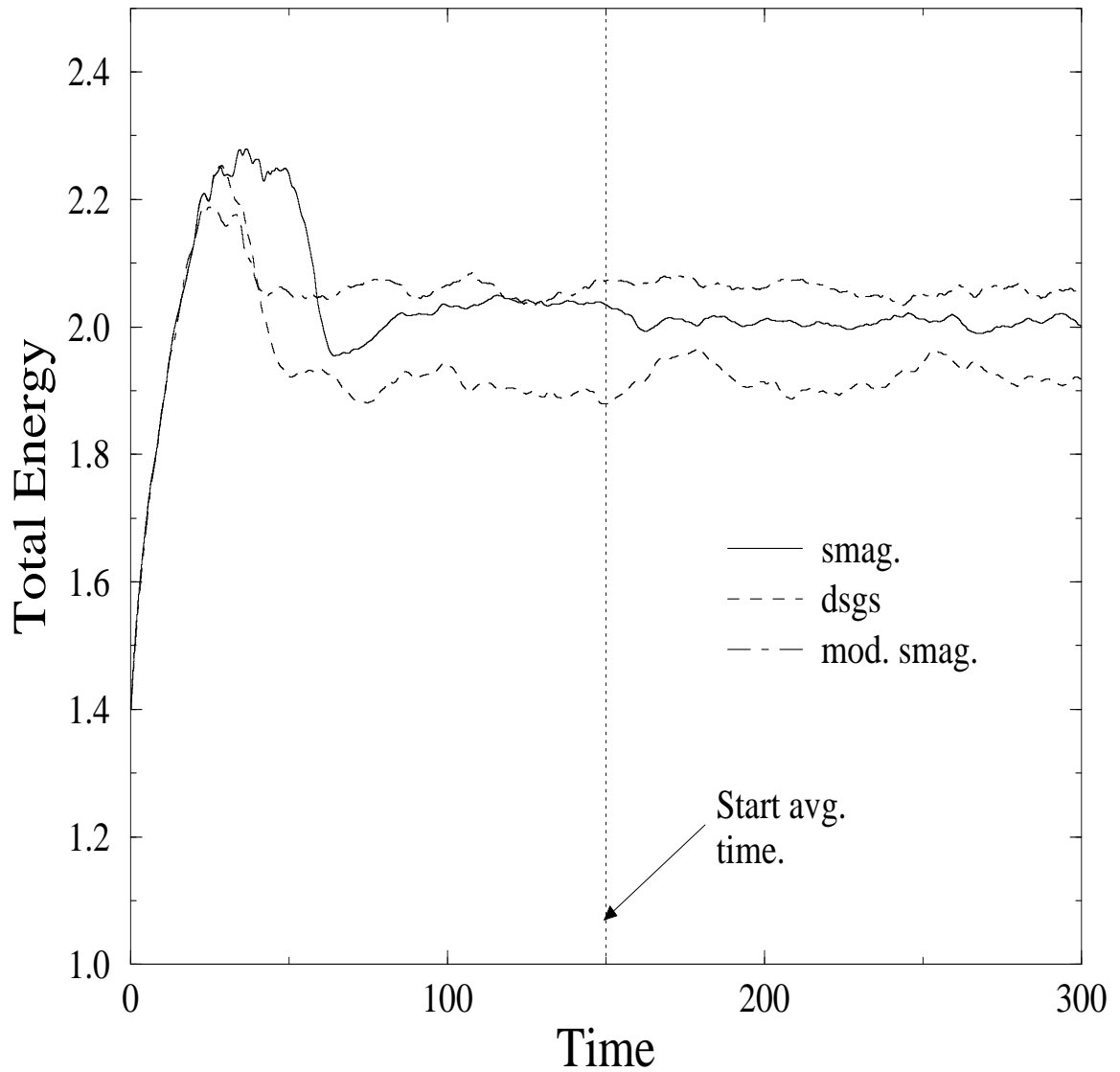


Figure 15: Plot of the total kinetic energy for the backward facing step using the Smagorinsky, DSGS, and modified Smagorinsky subgrid scale models. At time  $t = 150$ , a running total of the fluid variables is started to calculate the various mean properties of the flow.

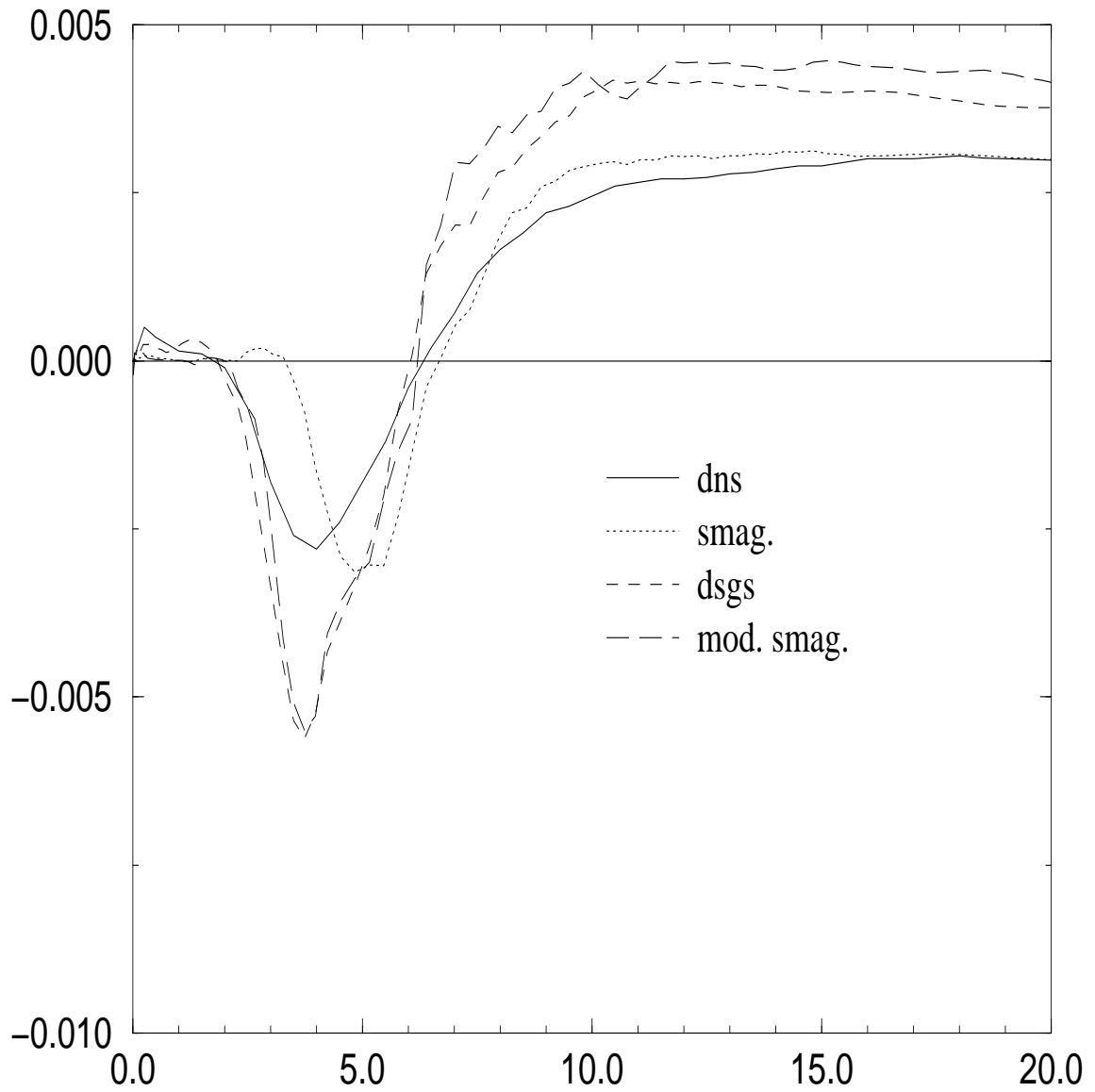


Figure 16: *Skin friction coefficient along the bottom wall of the post expansion section of the backward facing step problem. dns: direct numerical simulation data of Le and Moin [15], smag.: original Smagorinsky subgrid scale model, dsgs: dynamic subgrid scale model, and mod. smag.: modified Smagorinsky model.*



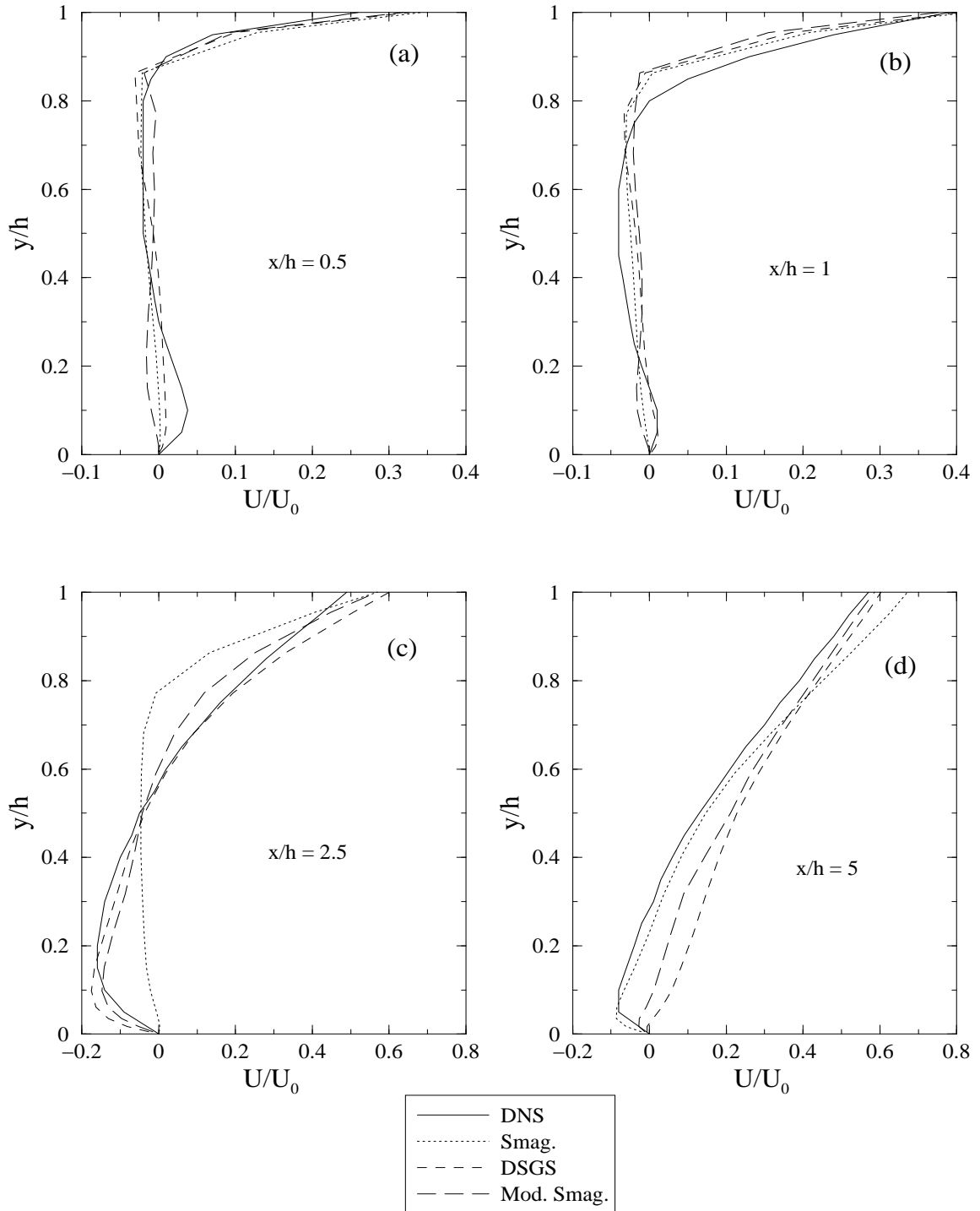


Figure 17: Mean streamwise velocity profiles in the post expansion section of the backward facing step problem. dns: direct numerical simulation data of Le and Moin [15], smag.: original Smagorinsky subgrid scale model, dsgs: dynamic subgrid scale model, and mod. smag.: modified Smagorinsky model.

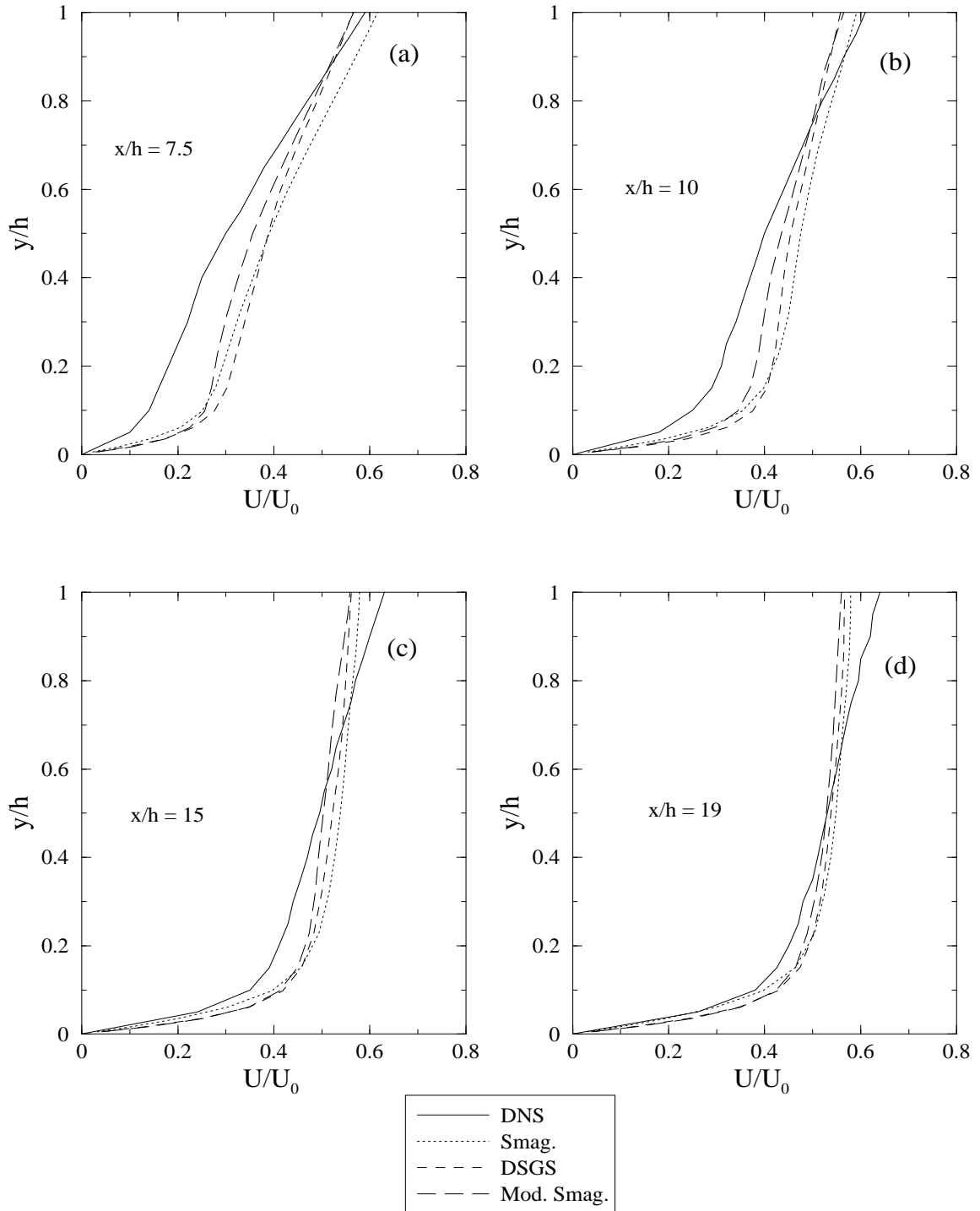


Figure 18: Mean streamwise velocity profiles in the post expansion section of the backward facing step problem. dns: direct numerical simulation data of Le and Moin [15], smag.: original Smagorinsky subgrid scale model, dsGS: dynamic subgrid scale model, and mod. smag.: modified Smagorinsky model.

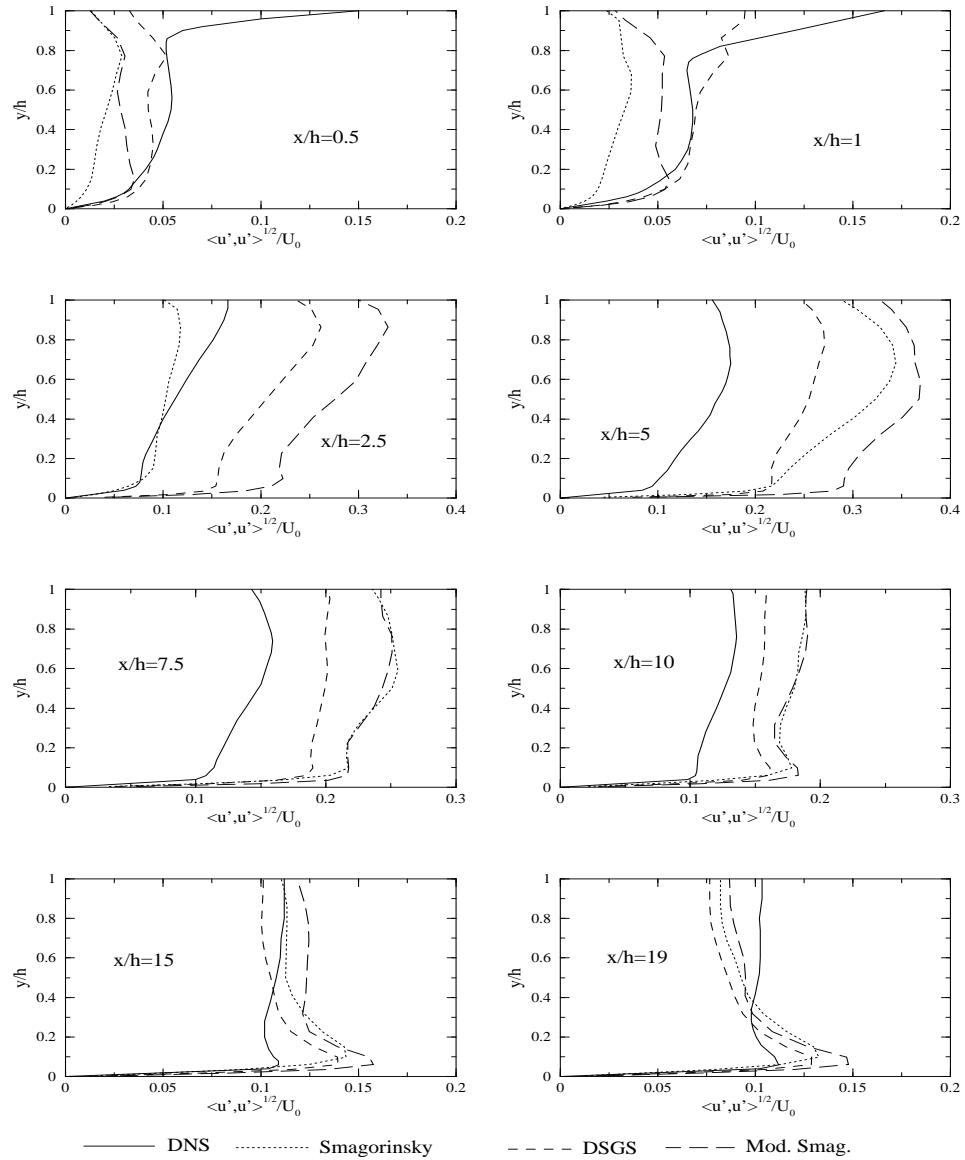


Figure 19: *Streamwise turbulence intensity profiles in the post expansion section of the backward facing step problem. DNS: direct numerical simulation data of Le and Moin [15], Smagorinsky: original Smagorinsky subgrid scale model, DSGS: dynamic subgrid scale model, and Mod. Smagorinsky: modified Smagorinsky model.*

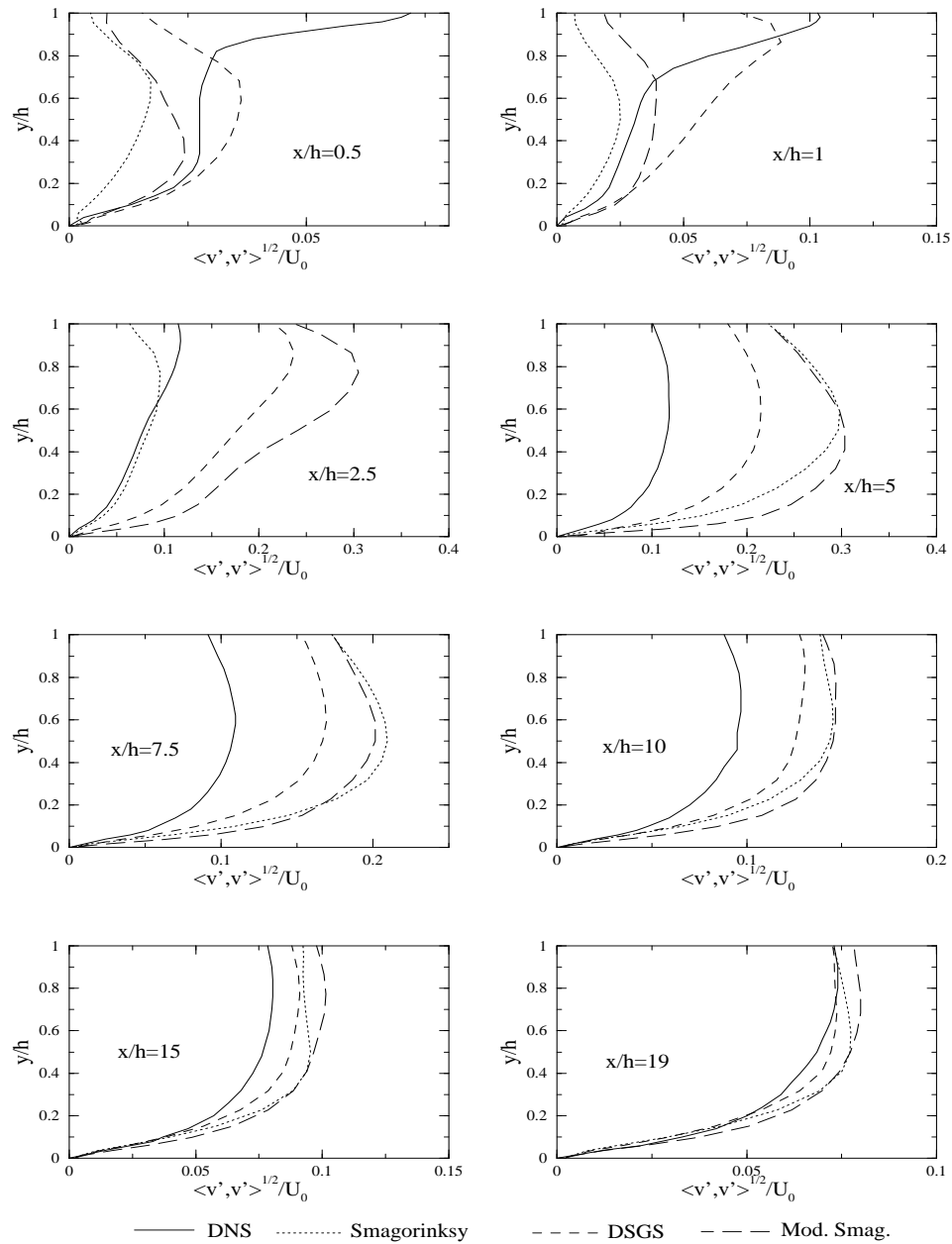


Figure 20: Wall normal turbulence intensity profiles in the post expansion section of the backward facing step problem. DNS: direct numerical simulation data of Le and Moin [15], Smagorinsky: original Smagorinsky subgrid scale model, DSGS: dynamic subgrid scale model, and Mod. Smagorinsky: modified Smagorinsky model.

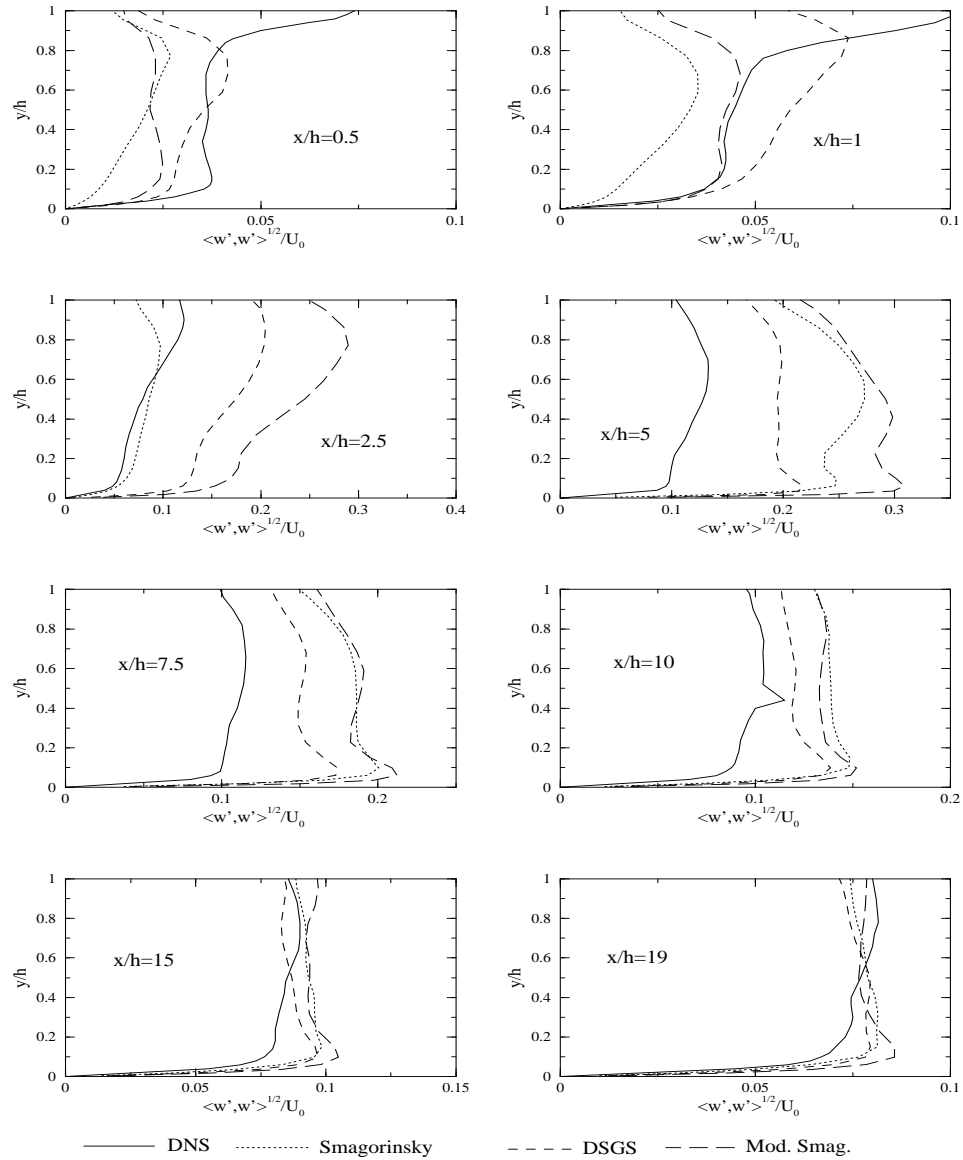


Figure 21: *Spanwise turbulence intensity profiles in the post expansion section of the backward facing step problem. DNS: direct numerical simulation data of Le and Moin [15], Smagorinsky: original Smagorinsky subgrid scale model, DSGS: dynamic subgrid scale model, and Mod. Smagorinsky: modified Smagorinsky model.*

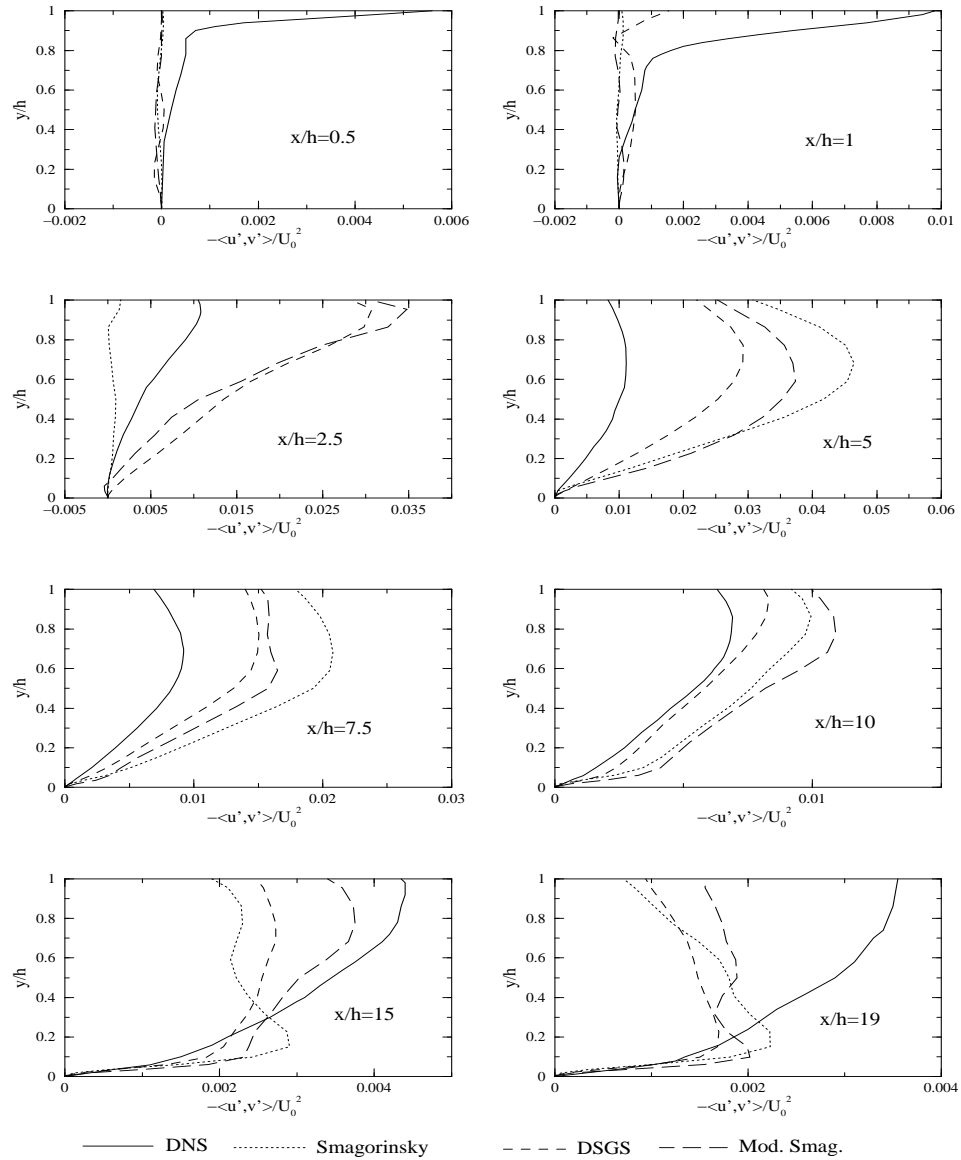


Figure 22: Reynolds shear stress profiles in the post expansion section of the backward facing step problem. DNS: direct numerical simulation data of Le and Moin [15], Smagorinsky: original Smagorinsky subgrid scale model, DSGS: dynamic subgrid scale model, and Mod. Smagorinsky: modified Smagorinsky model.

## 5 Computer Software

The numerical package used in this study is known as Hydra. This software was developed by Mark Christon for Lawrence Livermore National Laboratory. The finite element code was in turn developed on the works of Gresho et al. [9], [10], [8]. The original Smagorinsky turbulence model was incorporated into the code based on the work of Rose McCallen. Also a discussion of the motivation for using the finite element method is also presented by McCallen [19].

Although Hydra has several options for solving the Pressure Poisson Equation, it was found that for our turbulent flow cases the only solver that worked within a reasonable period of time was a version of the direct solver. This together with our limited computer resources restricted our mesh size to the  $88 \times 32 \times 16$  grid that was used for the above results.

## 6 Conclusions

One of the unique characteristics of LES as compared to other methods of dealing with turbulent flows is the idea of filtering. As was mentioned before, this concept of filtering introduces a new error to the system which is the result of the noncommutative nature of the filtering operation and differentiation in graded computational grids. Most of the focus in studying this error has been on the filter kernel function  $G$  and trying to obtain a  $G$  that would allow control over the order of the interchange error. As we used FEM as our numerical method, we had knowledge of the general shape of the solution (element wise) and so decided to focus on trying to use this extra information. We were able to show that under certain conditions the interchange error is second order.

As we have noted previously, one of the weaknesses of the Smagorinsky subgrid scale model is its inability to damp out the eddy viscosity near walls. The purpose of this project was to develop and implement a new subgrid scale model that would address this problem. To test the new model two turbulent flows were studied, the channel flow and the backward facing step. The channel flow was chosen because of the extensive amount of data, experimental, computational, and analytical, that is available for that type of flow. The backward facing step was chosen because of its geometric simplicity for a flow with separation and reattachment. Also, the Smagorinsky and a version of the Dynamic Subgrid Scale model were also implemented for comparison. These two models were chosen for comparison for two reasons. First, they



represent the two SGS models that are in common use in LES and secondly, their treatment of the eddy viscosity near walls are very different. As mentioned above, the Smagorinsky model does not damp out the eddy viscosity near the walls whereas the DSGS model does damp them out. Although the DSGS model does damp out eddy viscosity near the walls, some problems with the model, as mentioned previously, are that it requires double filtering and the eddy viscosity becomes negative and leads to numerical instability if left unchecked.

The results of our computations with the modified Smagorinsky model were comparable to the DSGS model computations and generally performed better than the original Smagorinsky model. Our eddy viscosity data from the channel flow indicate that our model and the DSGS were indeed able to detect the walls of the channel and reduce the eddy viscosity accordingly.

The next step in the continuation of this work should be to develop a better numerical solver that would allow a finer grid and, in the case of the backward facing step, allow an inlet channel to also be used.

## References

- [1] Knut Akselvoll and Parviz Moin. Large eddy simulation of turbulent confined coannular jets and turbulent flow over a backward facing step. Technical Report TF-63, Thermosciences Div., Dept. of Mech. Engr., Stanford Univ., February 1995.
- [2] J. W. Deardorff. A numerical study of three-dimensional turbulent channel flow at large reynolds numbers. *J. Fluid Mech.*, 41:453 – 480, 1970.
- [3] H. Eckelmann. The structure of the viscous sublayer and the adjacent wall region in a turbulent channel flow. *J. Fluid Mech.*, 65:439, 1974.
- [4] Joel H. Ferziger. Large eddy simulation. In Thomas B. Gatski, M. Yousuff Hussaini, and John L. Lumley, editors, *Simulation and Modeling of Turbulent Flows*, ICASE/LaRC Series in Computational Science and Engineering. Oxford University Press, 1996.
- [5] M. Germano. Differential filters for the large eddy numerical simulation of turbulent flows. *Phys. Fluids*, 29:1755 – 1758, June 1986.
- [6] Massimo Germano, Ugo Piomelli, Parviz Moin, and William Cabot. A dynamic subgrid-scale eddy viscosity model. *Phys. Fluids*, 3:1760 – 1765, July 1991.
- [7] S. Ghosal and P. Moin. The basic equations for the large eddy simulation of turbulent flows in complex geometry. *J. of Computational Physics.*, 118:24 – 37, 1995.
- [8] Philip M. Gresho. On the theory of semi-implicit projection methods for viscous incompressible flow and its implementation via a finite element method that also introduces a nearly consistent mass matrix. *Int. J. for Numerical Methods in Fluids*, 11:587 – 620, 1990.
- [9] Philip M. Gresho, Stevens T. Chan, Robert L. Lee, and Craig D. Upson. A modified finite element method for solving the time-dependent, incompressible navier–stokes equations. part 1: Theory. *Int. J. for Numerical Methods in Fluids*, 4:557 – 598, 1984.
- [10] Philip M. Gresho, Stevens T. Chan, Robert L. Lee, and Craig D. Upson. A modified finite element method for solving the time-dependent, incompressible navier–stokes equations. part 2: Application. *Int. J. for Numerical Methods in Fluids*, 4:619 – 640, 1984.
- [11] S. Jovic and D. M. Driver. Backward-facing step measurement at low reynolds number,  $re_h = 5000$ . NASA Technical Memorandum, 1994. No. 108807.

- [12] John Kim, Parviz Moin, and Robert Moser. Turbulence statistics in fully developed channel flow at low reynolds number. *J. Fluid Mech.*, 177:133 – 166, 1987.
- [13] H. Kreplin and H. Eckelmann. Behavior of the three fluctuating velocity components in the wall region of a turbulent channel flow. *Phys. Fluids*, 22:1233, 1979.
- [14] D. Kwak, W.C. Reynolds, and J.H. Ferziger. Three-dimensional time dependent computation of turbulent flow. Technical Report TF-5, Thermosciences Div., Dept. of Mech. Engr., Stanford Univ., May 1975.
- [15] Hung Le and Parviz Moin. Direct numerical simulation of turbulent flow over a backward facing step. Technical Report TF-58, Thermosciences Div., Dept. of Mech. Engr., Stanford Univ., December 1994.
- [16] A. Leonard. Energy cascade in large-eddy simulations of turbulent fluid flows. *Adv. Geophys.*, 18A:237 – 248, 1974.
- [17] A. L. Marsden, O. V. Vasilyev, and P. Moin. Construction of commutative filters for les on unstructured meshes. Center for Turbulence Research. Annual Research Briefs 2000.
- [18] P. J. Mason. Large-eddy simulation of turbulent shear flows. *von Karman Institute lecture series*, 1989–03, February 1989.
- [19] Rose C. McCallen. *Large-Eddy simulation of turbulent flow using the finite element method*. PhD thesis, U.C. Davis, 1993.
- [20] Charles Meneveau, Thomas Lund, and William Cabot. A lagrangian dynamic subgrid-scale model of turbulence. *J. Fluid Mech.*, 319:353 – 385, 1996.
- [21] F. M. Najjar and D. K. Tafti. Study of discrete test filters and finite difference approximations for the dynamic subgrid-scale stress model. *Phys. Fluids*, 8:1076 – 1088, April 1996.
- [22] Ugo Piomelli, William Cabot, Parviz Moin, and Sangsan Lee. Subgrid-scale backscatter in turbulent and transitional flows. *Phys. Fluids*, 3:1766 – 1771, July 1991.
- [23] Ugo Piomelli and Junhui Liu. Large-eddy simulation of rotating channel flows using a localized dynamic model. *Phys. Fluids*, 7:839 – 848, April 1995.
- [24] R. S. Rogallo and P. Moin. Numerical simulation of turbulent flows. *Ann. Rev. Fluid Mech.*, 16:99 – 137, 1984.

- [25] J. Smagorinsky. General circulation experiments with the primitive equations. *Monthly Weather Review*, 91(3):99 – 164, Mar 1963.
- [26] H. Tennekes and J. L. Lumley. *A First Course in Turbulence*. MIT Press, 1994.
- [27] Khoa Dang Tran and Yves Morchoisne. Numerical methods for direct simulation of turbulent shear flows. von Karman Institute for Fluid Dynamics Lecture Series, February 1989.
- [28] Harmen van der Ven. A family of large eddy simulation (les) filters with nonuniform filter widths. *Phys. Fluids*, 7:1171 – 1172, May 1995.
- [29] O. Vasilyev, T. S. Lund, and P. Moin. A general class of commutative filters for les in complex geometries. *J. of Computational Physics*, 146:82 – 104, Oct. 1998.
- [30] Oleg V. Vasilyev and Thomas S. Lund. A general theory of discrete filtering for les in complex geometry. Center for Turbulence Research, Stanford Univ. Annual Research Brief 1997.

## A Filter/Derivative Interchange Error

In this section we analyze the error in the interchange of filtering and differentiation by numerically calculating the filter of the derivative and the derivative of the filter and comparing the difference between the two. We begin by first creating our graded mesh. The mesh is generated by taking an interval  $[a, b]$ , in our case  $[0, 1]$ , and partitioning it into  $n$  even intervals. The graded mesh is then generated by using the following transformation:

$$x_i = \frac{e^{\alpha(a+ih)} - 1}{e^\alpha - 1}$$

where  $h = \frac{1}{n}$  and  $\alpha$  is some constant, which in our case is  $\alpha = 5$ . If we define the filter width,  $\Delta(x)$ , to be twice the length of the smallest element containing  $x$ , then we have

$$\begin{aligned} \Delta(x_i) &= 2(x_i - x_{i-1}) \\ &= 2 \left[ \frac{e^{\alpha(a+ih)} - 1}{e^\alpha - 1} - \frac{e^{\alpha(a+(i-1)h)} - 1}{e^\alpha - 1} \right] \\ &= 2 \left[ \frac{e^{\alpha(a+ih)}(1 - e^{-\alpha h})}{e^\alpha - 1} \right] \\ &= 2 \left[ \frac{(e^{\alpha(a+ih)} - 1 + 1)(1 - e^{-\alpha h})}{e^\alpha - 1} \right] \\ &= 2 \left[ x_i(1 - e^{-\alpha h}) + \frac{1 - e^{-\alpha h}}{e^\alpha - 1} \right]. \end{aligned}$$

So

$$\Delta(x) = 2 \left[ x(1 - e^{-\alpha h}) + \frac{1 - e^{-\alpha h}}{e^\alpha - 1} \right] \quad (25)$$

and

$$\Delta'(x) = 2(1 - e^{-\alpha h}). \quad (26)$$

Taking the Taylor expansion of the exponential function about 0 in Eqn. (25) and (26), it is clear that the order of the filter width and its derivative is  $h$ , i. e.  $O(\Delta(x)) = O(\Delta'(x)) = O(h)$ .

The numerical differentiation is performed using a fourth order method and the integration is carried out using the Composite Simpson's Rule over each element in the filter support. This ensures that the numerical integration is also at least fourth order in  $h$ . We use a truncated Gaussian as our filter and two different filter widths were tested,  $\Delta_1(x_i) = 2(x_i - x_{i-1})$  and  $\Delta_2(x_i) = 2(x_i - x_{i-2})$ .

To test the validity of our assertion that the numerical differentiation and integration methods used are in fact fourth order, we observe the following. In section 2.2, page 11 we found the interchange error to be

$$\left| \frac{d\bar{u}}{dx}(x) - \overline{\frac{du}{dx}}(x) \right| = \left| \Delta'(x) \int_{-\frac{1}{2}}^{\frac{1}{2}} yG(y)u'_e(x - y\Delta(x)) dy \right|.$$

Note that if our original function is a line, e. g.  $u(x) = 10x + 1$ , then our polynomial interpolations will all be exact, i. e.  $u_e(x) = u(x)$  everywhere. Furthermore, the derivative is constant and the same in every element, e. g. for the above linear  $u$ ,  $u'_e(x) = 10$ . So the interchange error should be 0. Hence the only error observed with the linear  $u$  will be the error in the calculation of the derivatives and integrals. Table 1 indicates fourth order behavior and so our claim of fourth order accuracy of the numerical differentiation and integration is justified.

We test the interchange error by using a sinusoidal source function

$$u(x) = \sin(2\pi x) + 1.$$

Table 2 clearly indicates that the interchange error is second order. Hence our claim that the interchange error is second order if  $O(\Delta'(x)) = O(\Delta(x))$  is justified.

$\left\  \frac{d\bar{u}}{dx}(x) - \overline{\frac{du}{dx}}(x) \right\ _{\infty}$				
	linear interpolation		quadratic interpolation	
h	$\Delta_1(x)$	$\Delta_2(x)$	$\Delta_1(x)$	$\Delta_2(x)$
0.05	1.20e-03	1.20e-03	1.20e-03	1.20e-03
0.005	1.19e-07	1.06e-07	1.19e-07	1.06e-07
0.0005	1.72e-10	1.68e-10	1.70e-10	1.68e-10

Table 1: Max norm of the diff./filter interchange error, linear source function  $u(x) = 10x + 1$

$\left\  \frac{d\bar{u}}{dx}(x) - \overline{\frac{du}{dx}}(x) \right\ _{\infty}$				
	linear interpolation		quadratic interpolation	
h	$\Delta_1(x)$	$\Delta_2(x)$	$\Delta_1(x)$	$\Delta_2(x)$
0.01	1.07e-02	4.31e-02	1.37e-02	4.94e-02
0.001	1.20e-04	4.97e-04	1.55e-04	6.13e-04
0.0001	1.60e-06	5.00e-06	1.56e-06	6.18e-06

Table 2: Max norm of the diff./filter interchange error, sine source function  $u(x) = \sin(2\pi x) + 1$



## B The Effect of Double Filtering

The following is a verification of the assumption, in Germano's derivation of his Dynamic Subgrid Scale Model, that filtering twice is equivalent to filtering once with some filter. In this paper we look at two filters that are often mentioned with regard to LES. Namely the Gaussian filter and the Top-Hat filter.

### B.1 Gaussian Filter

Given a Gaussian function

$$G(t) = e^{-\alpha t^2} = \frac{1}{2\pi} \int G(k) e^{ikt} dk$$

the Fourier Transform of  $G(t)$  denoted as  $G(k)$  is

$$G(k) = \sqrt{\frac{\pi}{\alpha}} e^{-\frac{k^2}{4\alpha}} = \int G(t) e^{-ikt} dt$$

Now we look at the following integral,

$$\bar{u}(x) = \int u(\xi) G(x - \xi) d\xi = u(x) * G(x)$$

which is a more general case of the familiar Gaussian filter in LES. It will be easier to insert the parameters later to change this into the proper Gaussian filter. Let

$$G_1(t) = e^{-\alpha_1 t^2}$$

and

$$G_2(t) = e^{-\alpha_2 t^2}$$

then we define

$$\bar{u}(x) = \int u(\xi)G_1(x - \xi)d\xi = u(x) * G_1(x)$$

and

$$\tilde{u}(x) = \bar{u}(x) * G_2(x)$$

So the Time Convolution Theorem, which states that the Fourier Transform of the convolution of two functions is equal to the product of the Fourier Transform of each of the functions, gives us

$$\bar{u}(k) = u(k)G_1(k)$$

and

$$\begin{aligned} \tilde{u}(k) &= \bar{u}(k)G_2(k) \\ &= u(k)G_1(k)G_2(k) \\ &= \frac{\pi}{\sqrt{\alpha_1\alpha_2}}u(k)e^{\frac{-k^2}{4}\left(\frac{1}{\alpha_1}+\frac{1}{\alpha_2}\right)} \end{aligned}$$

Hence using the inverse transform, we get

$$\begin{aligned} \tilde{u}(x) &= \frac{\pi}{\sqrt{\alpha_1\alpha_2}}\frac{1}{2\pi}\int u(k)e^{\frac{-k^2}{4}\left(\frac{1}{\alpha_1}+\frac{1}{\alpha_2}\right)}e^{ikx}dk \\ &= \frac{\pi}{\sqrt{\alpha_1\alpha_2}}\frac{1}{2\pi}\int e^{\frac{-k^2}{4}\left(\frac{1}{\alpha_1}+\frac{1}{\alpha_2}\right)}e^{ikx}\int u(\xi)e^{-ik\xi}d\xi dk \\ &= \frac{1}{2\sqrt{\alpha_1\alpha_2}}\int u(\xi)\int e^{\frac{-k^2}{4}\left(\frac{1}{\alpha_1}+\frac{1}{\alpha_2}\right)}e^{ik(x-\xi)}dkd\xi \end{aligned}$$

Now if we let

$$\frac{1}{\alpha_3} = \frac{1}{\alpha_1} + \frac{1}{\alpha_2}$$

so

$$\alpha_3 = \frac{\alpha_1 \alpha_2}{\alpha_1 + \alpha_2}$$

and

$$G_3(x) = e^{-\alpha_3 x^2} = \frac{1}{2\pi} \int G_3(k) e^{ikx} dk$$

then

$$G_3(k) = \sqrt{\frac{\pi}{\alpha_3}} e^{-\frac{k^2}{4\alpha_3}}$$

So

$$\begin{aligned} \tilde{u}(x) &= \frac{1}{2\sqrt{\alpha_1 \alpha_2}} \int u(\xi) \int e^{\frac{-k^2}{4} \left( \frac{1}{\alpha_1} + \frac{1}{\alpha_2} \right)} e^{ik(x-\xi)} dk d\xi \\ &= \frac{1}{2\sqrt{\pi} \sqrt{\alpha_1 + \alpha_2}} \int u(\xi) \int G_3(k) e^{ik(x-\xi)} dk d\xi \\ &= \sqrt{\frac{\pi}{\alpha_1 + \alpha_2}} \int u(\xi) G_3(x - \xi) d\xi \\ &= \sqrt{\frac{\pi}{\alpha_1 + \alpha_2}} \int u(\xi) e^{-(x-\xi)^2 \alpha} d\xi \end{aligned}$$

Now the Gaussian filter for LES is

$$G(x) = \sqrt{\frac{6}{\pi}} \frac{1}{\Delta} e^{-6 \frac{x^2}{\Delta^2}}$$

So if we let

$$G_1(x) = \sqrt{\frac{6}{\pi}} \frac{1}{\Delta_1} e^{-6 \frac{x^2}{\Delta_1^2}}$$

$$G_2(x) = \sqrt{\frac{6}{\pi}} \frac{1}{\Delta_2} e^{-6 \frac{x^2}{\Delta_2^2}}$$

then  $\alpha_1 = \frac{6}{\Delta_1^2}$ ,  $\alpha_2 = \frac{6}{\Delta_2^2}$  and  $\alpha_3 = \frac{6}{\Delta_1^2 + \Delta_2^2}$ . Hence if we go back and let  $\bar{\cdot}$  and  $\tilde{\cdot}$  be the proper Gaussian filters defined with the above kernels, we have that

$$\begin{aligned} \tilde{u}(x) &= [u(x) * G_1(x)] * G_2(x) \\ &= \frac{6}{\pi} \frac{\sqrt{\pi}}{\Delta_1 \Delta_2} \frac{\Delta_1 \Delta_2}{\sqrt{6(\Delta_1^2 + \Delta_2^2)}} \int u(\xi) e^{-\frac{(x-\xi)^2}{\Delta_1^2 + \Delta_2^2}} d\xi \\ &= \sqrt{\frac{6}{\pi}} \frac{1}{\sqrt{\Delta_1^2 + \Delta_2^2}} \int u(\xi) e^{-6\frac{(x-\xi)^2}{\Delta_1^2 + \Delta_2^2}} d\xi \\ &= u(x) * G_s(x) \end{aligned}$$

where  $G_s(x)$  is the Gaussian filter with filter width  $\Delta = \sqrt{\Delta_1^2 + \Delta_2^2}$ .

## B.2 Top-Hat Filter

The Top-Hat filter is defined as

$$p_{\frac{\Delta}{2}}(x) = \begin{cases} \frac{1}{\Delta} & : |x| < \frac{\Delta}{2} \\ 0 & : \text{otherwise} \end{cases}$$

We also define a triangle filter as follows.

$$q_{\Delta}(x) = \frac{1}{\Delta} \begin{cases} 1 + \frac{x}{\Delta} & : -\Delta < x < 0 \\ 1 - \frac{x}{\Delta} & : 0 < x < \Delta \\ 0 & : \text{otherwise} \end{cases}$$

Now the Fourier Transform of the above functions are

$$p_{\frac{\Delta}{2}}(k) = \frac{2 \sin(\frac{k\Delta}{2})}{k\Delta}$$

and

$$q_{\Delta}(k) = \frac{4 \sin^2(\frac{k\Delta}{2})}{\Delta^2 k^2}$$

If we define  $\bar{\cdot}$  to be the Top-Hat filter and  $\tilde{\cdot}$  to be the triangle filter, then note that if we filter twice with the same (width) Top-Hat filter we get

$$\overline{\overline{u}}(x) = u * p_{\frac{\Delta}{2}} * p_{\frac{\Delta}{2}}$$

So the Fourier Transform of  $\overline{\overline{u}}$  is

$$\begin{aligned} \overline{\overline{u}}(k) &= u(k)p_{\frac{\Delta}{2}}(k)p_{\frac{\Delta}{2}}(k) \\ &= u(k)\frac{4\sin^2(\frac{k\Delta}{2})}{k^2\Delta^2} \end{aligned}$$

Hence

$$\begin{aligned} \overline{\overline{u}}(x) &= \frac{1}{2\pi} \int \overline{\overline{u}}(k)e^{ikx} dk \\ &= \frac{1}{2\pi\Delta^2} \int \frac{4\sin^2(\frac{k\Delta}{2})}{k^2} e^{ikx} \int u(\xi)e^{-ik\xi} d\xi dk \\ &= \frac{1}{2\pi\Delta^2} \int u(\xi) \int \frac{4\sin^2(\frac{k\Delta}{2})}{k^2} e^{ik(x-\xi)} dk d\xi \\ &= \frac{1}{\Delta} \int u(\xi) \frac{1}{2\pi} \int \frac{4\sin^2(\frac{k\Delta}{2})}{\Delta^2 k^2} e^{ik(x-\xi)} dk d\xi \\ &= \frac{1}{\Delta} \int u(\xi) q_{\Delta}(x-\xi) d\xi \\ &= \tilde{u}(x) \end{aligned}$$

where

$$q_{\Delta}(x-\xi) = \frac{1}{\Delta} \begin{cases} 1 + \frac{\xi-x}{\Delta} & : x - \Delta < \xi < x \\ 1 - \frac{\xi-x}{\Delta} & : x < \xi < x + \Delta \\ 0 & : \text{otherwise} \end{cases}$$

So filtering with the same Top-Hat filter twice is equivalent to filtering once with the triangle filter,  $q_{\Delta}$ .

# A Modified Smagorinsky Subgrid Scale Model for the Large Eddy Simulation of Turbulent Flow

BY

Tommy Kunhung Kim

B.A. (California State University, Fullerton) 1990  
M.A. (California State University, Fullerton) 1992

DISSERTATION

Submitted in partial satisfaction of the requirements for the degree of

DOCTOR OF PHILOSOPHY

in

Applied Mathematics

in the

OFFICE OF GRADUATE STUDIES

of the

UNIVERSITY OF CALIFORNIA

DAVIS

Advisor: Dr. Wolfgang Kollmann

2001